A 2D Simulation Methodology for Thermo-Magnetics Effects on Tunneling Mechanisms of Nano-scaled MOS Devices

by

Gabriela Alejandra Rodríguez Ruiz

A dissertation submitted to the Electronics Department in partial fulfillment of the requirements for the degree of

D.Sc. in Electronics

at the

National Institute for Astrophysics, Optics and Electronics

February 2015

Tonantzintla, Puebla

Advisors:

Dr. Librado Arturo Sarmiento Reyes
Dr. Edmundo Antonio Gutiérrez Domínguez

Abstract

The development of a 2D numerical simulation methodology that accounts for thermal and magnetic effects on the gate tunneling current of nano-scaled MOSFETs, is the main goal of this thesis. The Schrödinger-Poisson coupled equation system is modified to account for the influence of a static magnetic field. The wavefunctions, which are the solution to the Schrödinger-Poisson coupled equation system, and the energy, are then obtained as a function of the magnetic field and temperature. Then, by considering open boundary conditions with the Perfectly Matched Layer-PML method and using the Tsu-Esaki direct tunneling model, the gate tunneling current under the influence of a magnetic field and temperature is calculated. By modifying the source files of the commercial GTS Framework device simulation tool to incorporate the new simulation methodology, the gate tunneling current is computed as a function of electrical bias, temperature and magnetic field. By doing so, and by sweeping the magnetic field from negative to positive values, it is found out that electrical charges tunneling, through the gate oxide, from the semiconductor to the gate terminal, are swept from left to right. Therefore, the proposed simulation methodology, accompanied with experimental results, is a very valuable tool to investigate non-homogeneous space distributed tunneling properties.

Resumen

El desarrollo de una metodología de simulación numérica bi-dimensional que tome en cuenta efectos térmicos y magnéticos sobre la corriente de tuneleo de compuerta de MOSFETs nanométricos, es el principal objetivo de esta tesis. El sistema de ecuaciones acopladas de Schrödinger-Poisson se modificó para tomar en cuenta la influencia de un campo magnético estático. Las funciones de onda y las energías, las cuales son la solución del sistema de ecuaciones Schrödinger-Poisson, se obtienen como una función del campo magnético y de la temperatura. Considerando condiciones de frontera abiertas mediante el método *Perfectly Matched Layer* PML y utilizando el modelo de tuneleo directo de Tsu-Esaki, la corriente de tuneleo de compuerta bajo los efectos del campo magnético aplicado y la temperatura es calculada.

Mediante la incorporación de la nueva metodología de simulación dentro de los archivos fuente de la herramienta comercial de simulación GTS Framework, la corriente de tuneleo de compuerta es calculada como una función de la polarización eléctrica, la temperatura y el campo magnético. Mediante este proceso, y haciendo un barrido del campo magnético de valores positivos a negativos, se encontró que el tuneleo de cargas eléctricas a través del óxido, desde el semiconductor hasta la compuerta es barrido de derecha a izquierda (de lado de la fuente al lado del drenaje), lo que equivale a hacer un mapeo del espacio o un escaneo de las propiedades de tuneleo. Debido a esto, la metodología de simulación propuesta, acompañada con resultados experimentales, es una herramienta muy valiosa para investigar las propiedades de tuneleo en espacios distribuidos no homogeneamente.

Acknowledgment

To Norberto and Fabiola,

To Jesús

Contents

List of Figures

Acronyms

CMOS - Complementary Metal-Oxide-Semiconductor.

DIBL- Drain Induced Barried Lowering.

DT - Direct Tunneling.

FDM - Finite Difference Method.

FEM - Finite Element Method.

FET - Field Effect Transistor.

FVM - Finite Volume Method.

FN - Fowler-Nordheim.

GTS - General TCAD Solutions.

IC - Integrated Circuits.

INAOE - Instituto Nacional de Arstrofsica, ptica y Electrnica.

ITRS - International Technology Roadmap for Semiconductors.

MOSFET - Metal-Oxide-Semiconductor Field-Effect Transistor.

PML - Perfectly Matched Layer.

SCE - Short Channel Effects.

TAT - Trap Assisted Tunneling.

TC - Transmission Coefficient.

VSP - Vienna SChrödinger-Poisson.

WKB - Wenztsel-Kramers-Brillouin.

Chapter 1

Introduction

1.1 Motivation

For more than four decades, the semiconductor industry has been commited to reduce the dimensions of the MOSFET with the aim to obtain a better performance, lower cost and higher density integration of integrated circuits. Nowadays, the dimensions of the MOSFET have evolved from micrometer scales to nanometer scales, where for instance the channel length of a MOSFET is in the order of tens of nanometers and the oxide thickness is less than two nanometers [1]. According to the International Technology Roadmap for Semiconductors (ITRS 2012) in 2022 the oxide thickness will be less than 0.9 nm [2].

Other characteristic, that has been applied since many years, is the mechanical strain on nano-scaled MOSFETs. Mechanical strain has been applied into nano-scaled MOSFETs to enhance the average carrier mobility and current drive capability. However, such a mechanical stress is not uniformly distributed on the channel plane, which results in a non-homogeneous channel plane conductive properties (Figure 1.1 and Figure 1.2) [3, 4]. A pure electrical characterization technique for measuring the gate tunneling current Ig only gives the average scalar value of the Ig current at the gate contact, giving no information about the non-homogeneous space distributed conductive properties in nano-scaled MOSFET.

Recently, a new magnetic-electrical combined characterization technique for analyzing electrical and conductive properties of nano-scaled MOSFETs with ultra thin gate oxides
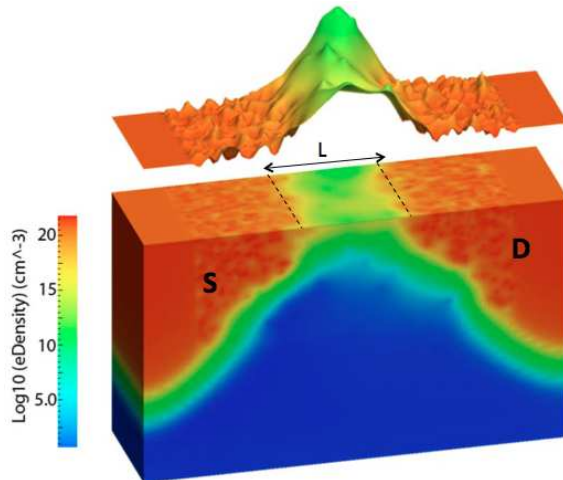
Figure 1.1: Simulation of the electron density distribution of a 35-nm MOSFET. [4]

has been developed at INAOE [5]. This alternative technique is based on the application of a magnetic field $\vec{B}$, which allows the electron flow to be deflected through regions with different conductivities. Then, by measuring the average current, under different magnetic flux magnitudes and directions, the conductivity can be scanned or mapped through different regions of the MOSFET channel [6]. Unlike a pure electrical characterization technique, this new electro-magnetic technique gives more information about the local space distribution of conductive properties of the MOSFET and proves to be effective to detect inhomogeneous tunneling properties along the channel of a MOSFET; a phenomenon that cannot be explained by resorting to purely electrical test techniques.

As the alternative characterization technique makes use of an externally applied magnetic field, there is the need to incorporate the magnetic field variable in a simulation tool. However, until now, there is no simulation tool that allows to incorporate electromagnetic effects in nano-scaled MOSFET simulations. In fact, this is introduced in this work, namely the incorporation of the magnetic field variable is done in addition of the temperature, so thermo-magnetic simulations can be performed in nano-scaled MOSFETs.

In this thesis, a preliminary modeling approach for simulating the electrical behavior of a nano-scaled MOSFET under the influence of an external magnetic field and thermal variations is proposed. As a first developing stage, a 2D modeling approach based on the
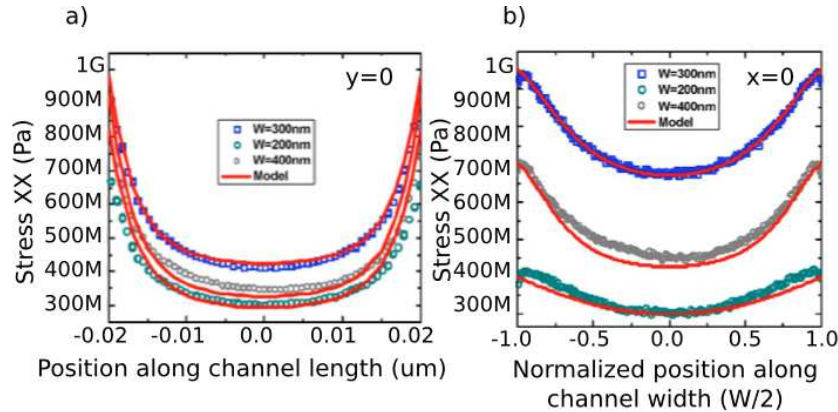
Figure 1.2: Simulation of the stress distribution along the channel length L (a) and along the width W (b) directions [3]

Schrödinger-Poisson system that incorporates the magnetic field and allow us to simulate the gate tunneling current of a MOSFET under the influence of a magnetic field and thermal variations is introduced.

1.2 Objectives

The main objective of this thesis is to develop a 2D simulation methodology for analyzing the gate tunneling current of nano-scaled MOSFETs under the influence of a static magnetic field. In order to achieve this general objective, the next particular objectives are proposed:

- Analyze, understand and modify the algorithm for the solution of the Schrödinger-Poisson system.

- Establish the appropiate boundary conditions.

- Incorporate the magnetic field into the model.

- Develop a methodology to compute the gate tunneling current of a MOSFET under the influence of a magnetic field.

- Incorporate the simulation methodology into the GTS Framework device simulator.

1.3 Structure of the thesis

This thesis is organized as follows, chapter 2 introduces the theoretical fundaments about gate tunneling current in nano-scaled MOSFETs and also shows a review of the state of the art of tunneling current simulation approaches. Chapter 3 presents the simulation methodology proposed in this thesis for simulating the gate tunneling current of nano-scaled MOSFETs under the influence of a magnetic field. Chapter 4 describes the experiments and results obtained with our simulator, and finally, in Chapter 5 the conclusions and future work are shown.

Chapter 2

Theoretical concepts

2.1   MOSFET scaling

The Metal-oxide-semiconductor Field-effect transistor (MOSFET) is one of the most used transistor in microelectronics industry, where more than 90% of all digital circuits are designed using the CMOS technology [7].

During the last four decades, the semiconductor industry has worked in the continuous reduction of MOSFET's dimensions to nanometer scales. The main reasons for pursuing miniaturization are the increment of packing density, chip functionality, lower costs and better performance of transistors (increment of current drive capability and speed). Following the Moore's law the number of transistors on IC doubles approximately every two years and according to the ITRS 2012 the channel length will be less than 9.0 nm and the oxide thickness will be less than 1.0 nm in 2022 [2]; (Figure 2.1).

Nevertheless, this scaling down process presents some important challenges to device design. The short channel effects (SCEs) and the gate tunneling current are some of the more important effects that reduce the performance of nano-scaled MOSFETs [9].

2.1.1   Short channel effects and gate tunneling current

- **Impact ionization.** The scaling down of MOSFETs dimensions produces high vertical and horizontal electric fields ($> 10^6 V/cm$). The rising in electric fields happens because
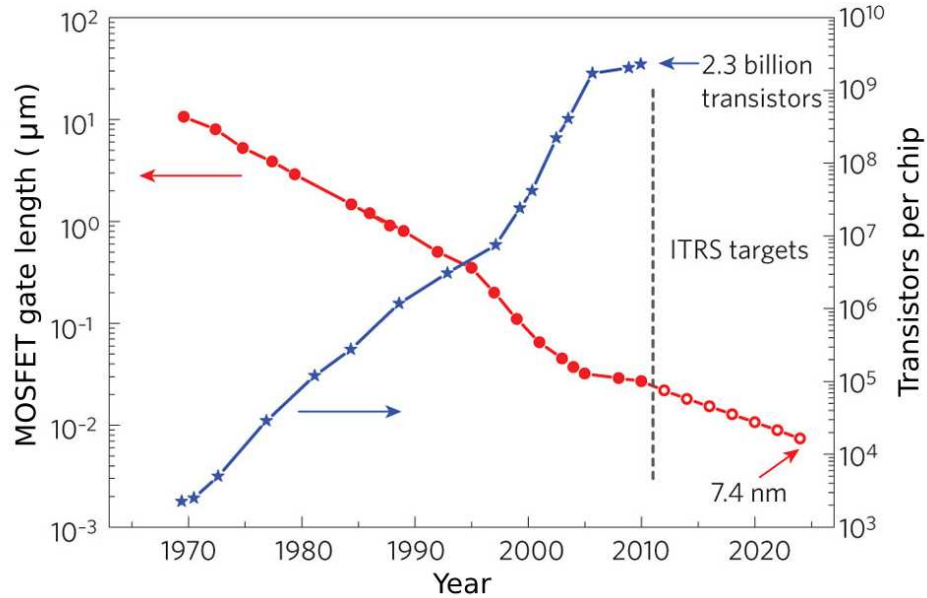
Figure 2.1: Evolution of MOSFET gate length (filled red circles) and International Technology Roadmap for Semiconductors (ITRS) targets (open red circles). Figure taken from [8]

.

the terminal voltages are not scaled down to maintain the speed of the MOSFET. Due to this reduction in size but not in voltage, short channel effects appear in nano-scaled MOSFETs. Due to the high intensity of the electric field near to the drain, the electrons have enough kinetic energy to hit a bounded electron and release it to the conduction band; which simultaneously produces an electron-hole pair. This process is called impact ionization and it produces electron-hole pairs in the silicon lattice causing even more ionization in the semiconductor. As a direct consequence, there is an increase in the drain-source current and substrate current (Figure 2.2) [9, 10].
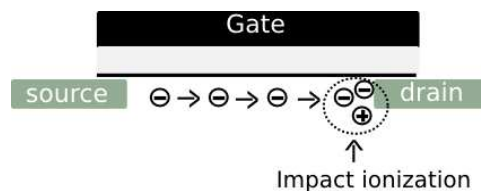
Figure 2.2: Impact ionization

.

- **Punch-Through and Drain Induced Barried Lowering (DIBL).** Due to the miniaturization of the channel length, the depletion region from drain can reach the source depletion region. The consequence of this, is the reduction of the barrier for electron injection and this effect is known as Punch-Through. In long channel devices, the semiconductor is depleted completely by the gate bias but in short channel devices, the semiconductor is depleted also by the source/drain bias. As the drain bias increases the depletion region is expanded and it can interact with the source/channel junction producing a lowering in the potential barrier (Figure 2.3 and Figure 2.4) [9].
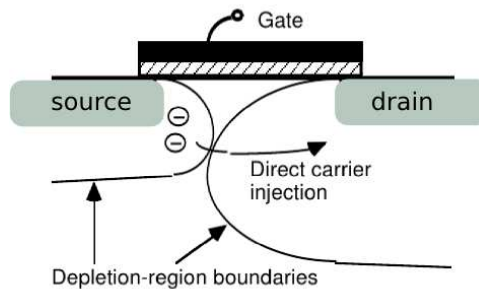
Figure 2.3: Punch-Through effect

.
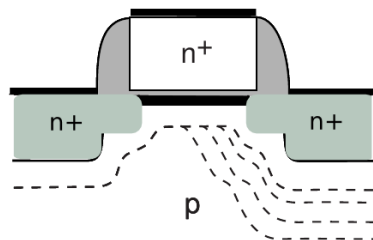
Figure 2.4: DIBL effect

.

- **Mobility reduction.** As the channel length is reduced, the lateral and vertical magnitude of electric fields are increased. As a result, the carrier velocity can be saturated and it produces a drecrease in the charge mobility [10].

- **Hot electron effect.** Due to the high electric field in nano-scaled MOSFET, electrons can acquire enough energy to pass over or tunneling the oxide barrier. Such electrons can become trapped in the oxide region, changing the threshold voltage of the device (Figure 2.5) [9].
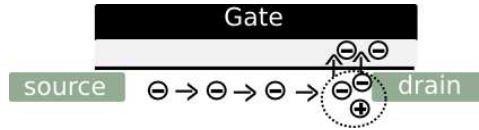
Figure 2.5: Hot electron effect

.

- **Gate tunneling current.**

  In nano-scaled MOSFETs, quantum effects as channel energy quantization and gate tunneling current dominate the electronic properties of the transistor. Due to the scaling down of MOSFETs dimensions, the oxide thickness is thinner than 2 nm, which causes an important flow of current through the gate. The oxide thickness is too thin that electrons can tunnel through the oxide barrier to the gate electrode. This tunneling current is one of the key leakage currents that contributes most to device degradation, leads to excessive power dissipation and loss of on-current density. Because of that, the reduction of leakage current is the main issue in MOSFET down scaling (Figure 2.6) [7, 9, 10].
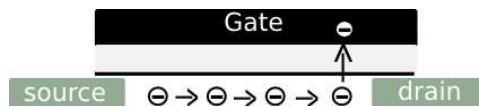
Figure 2.6: Gate tunneling current

.

2.2 Gate leakage current in MOSFETs

In nano-scaled MOSFETs, quantum effects as channel energy quantization and gate tunneling current dominate the electronic properties of the transistor [11]. Due to the aggresive scaling

down of the oxide thickness and the high electric fields produced by the high doping of channel, electrons can tunnel through the oxide barrier producing a high current flow, which results in a high power consumption in the off-state of the transistor. The gate tunneling current is one of the biggest limitations in the attempt to further reduce the size of transistors [12, 13].

This gate leakage current in MOSFETs is produced by different tunneling processes that are bias-dependent, and by thermal stress. The main three tunneling processes are the Fowler-Nordheim (FN), the Trap assisted tunneling (TAT) and the Direct tunneling (DT).

- **Fowler-Nordheim tunneling**

    In nMOS transistors, when a large positive voltage $(> 4V)$ is applied to the gate, the metal side of the band diagram is lowered enough so the potential barrier becomes approximately triangular (Figure 2.7). Due to this triangular potential barrier, electrons can easily tunnel from the conduction band of the semiconductor to the conduction band of the oxide. This tunneling process through an approximately triangular potential barrier is called Fowler-Nordheim tunneling. The simple expression for calculating the FN density current tunneling is

    $$J_{FN} = \frac{q^3 m_0}{16\pi^2 \hbar m_{ox} \phi_b} F^2 e^{-\beta/F}. \tag{2.1}$$

    Here $\hbar$ is the Planck's reduced constant, m_{ox} is the electron effective mass in the insulator, m_0 is the electron mass in free space, q is the electron charge, ϕ_b is the energy barrier height at the semiconductor-oxide interface, F is the electric field across the oxide, and $\beta = \frac{4(2m_{ox})^{1/2}}{3q\hbar} \phi_b^{3/2}$.

    The Fowler-Nordheim tunneling formula is very accurate for modeling gate tunneling current of MOSFETs with oxide thickness in the order of 7-10 nm [14].

- **Trap assisted tunneling**

    Defects in the insulator produce electronic states in the band gap of the oxide and can split the energy barrier into two parts, (Figure 2.8). These states allow the charge tun-
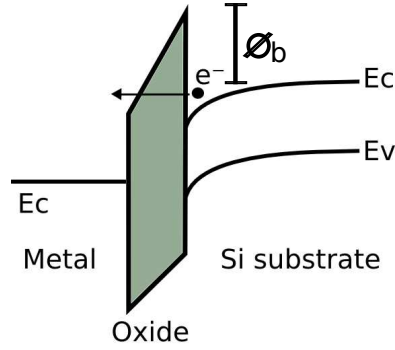
Figure 2.7: Fowler- Nordheim Tunneling (triangular barrier)

neling through thinner energy barriers. Electrons have a higher probability of tunneling in oxides with traps than those that tunnel the entire oxide. The basic model for the current density assited by traps J_{TAT} is [15]

$$J_{TAT} = q \int \frac{N_T}{\tau_c + \tau_e} \delta x, \tag{2.2}$$

where N_T is the trap density at a distance x away from the emitting electrode, τ_c characteristic times for carrier capture and τ_e is the characteristic times for emission by the trap.
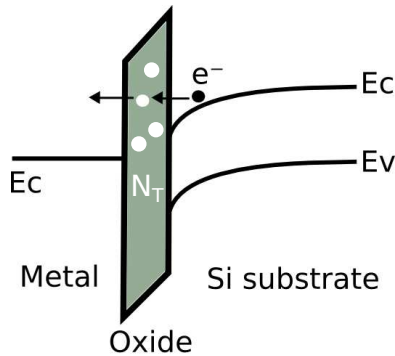
Figure 2.8: Trap assited tunneling

- **Direct tunneling**

  In ultra-thin oxide MOSFET (below 5nm), the strength of the electric field at the oxide is so high ($10^7 V/cm$) and the oxide is too thin ($< 5nm$) that electrons can tunnel in

a direct way through the barrier of the oxide. In this tunneling process, electrons can transverse the entire width of the potential barrier, even with lower applied voltage, and for this case the oxide potential profile is trapezoidal, (Figure 2.9).
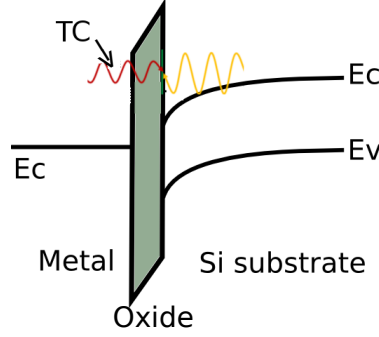
Figure 2.9: Direct Tunneling (trapezoidal barrier)

The tunneling probability increases drammatically as the oxide thickness is reduced [9]. This tunneling process is called direct tunneling and the electron flux from this tunneling process is the most dominant gate leakage process through oxides below 5nm [15], which is the case of a 28 nm CMOS transistor. Moreover, in order to model this effect, classical physics is not appropiate and quantum physics needs to be considered. The direct tunneling current can be described by the Tsu-Esaki formula [17],

$$J = \int_{E_{min}}^{E_{max}} TC(E_i)S(E_i)dE_x, \tag{2.3}$$

where S represents the number of electrons in an energy level, which are available for tunneling through the barrier potential function, the TC term is the transmission coefficient, E_x represents the electron kinetic energy in the direction perpendicular to the barrier.

Due to the impact of the direct tunneling current on the performance of nano-scaled MOSFETs with ultra-thin oxides, in this thesis we are particulary interested in modeling the direct tunneling (DT). In the next section a review of different modeling approaches for direct tunneling currents is introduced.

2.3 Literature Review of direct tunneling modeling

Since the scaling of gate oxide started in the 1970's, a lot of gate tunneling modeling approaches have been developed. In the 70's **Harrison** [16] and **Tsu** [17] proposed one of the first general direct tunneling current formula. The authors assume that the band structure varies slowly and the potential barrier has a triangular or trapezoidal shape. In order to calculate the transmission coefficient, they use the Wenztsel-Kramers-Brillouin (WKB) method [19]. The WKB method gives an approximation of the solution of the Schrödinger equation by means of an analytical formula, which depends on the width of the barrier. Such approximation method is accurate for triangular potential barriers. After that, **Rana et al.** [20] solved the self-consistent Schrödinger-Poisson system in one dimension for accumulation layers in MOS devices. The authors consider extended and quasi bound states for tunneling current. Moreover, they compare a semi-classical model with their model, obtaining almost the same current results. Then, **Lo et al.** [22] considered a tunneling current from the quantized states in the inversion layer of nano-scaled MOSFETs. The authors have calculated the lifetimes of quasi-bounded states and found that more than 80 percent of the total current comes from the lowest two energy states. The authors used the matrix-transfer method for calculating the transmission of the wavefunctions. The matrix-transfer method is used for calculating the transmission coefficient of a potential barrier. The method divides the potential barrier into a number of potential energy steps. By using a piecewise representation of the potential, the wavefunctions are approximated by constant values [23, 24]. In 1998, another work focused in the solution of the model in 1D was developed by **Janick and Majkusiak** [25]. These authors assumed a linear distribution of the potential (considering a system of decoupled equations Schrödinger-Poisson), rendering an analytical expression for the charge distribution. The Janick and Majkusiak's work considers a confined triangular well in a closed system. **Register et al.** [27] introduced an analytical model for direct tunneling gate current in MOSFETs. The analytical expression is based on the WKB method and the electric field on the surface. This method is accurate only for low electric fields ($< 10^6 V/cm$). **Mundanai et al.** [28] used a WKB approximation and obtained the tunneling current for different dielectrics materials and thicknesses. **Lee et al.** [30] used a modified WKB method

for calculating the direct tunneling current of MOS structures and investigated the effects on the direct tunneling current with different uniform doping concentrations in the substrate. In 2004, another important work was developed by **Driskill** [35]. This work computes the charge density and the tunneling current in a 1D quantum well. Moreover, Driskill assumes open boundary conditions, and calculates the tunneling current by means of the transfer matrix method and using finite difference method.

One of the first research groups, which solves the 2D Schrödinger-Poisson system, was the group of **Spinelli et al** [31] and the group of **Trellakis** [21]. In 2002, The authors solved a closed 2D Schrödinger-Poisson system using a finite element method. In order to calculate the current, they use a semiclassical approach, adopting a drift-diffusion model. After that, in 2003 the NANOTCAD2D simulator was developed by **Curatola et al** [32,33]. This simulator solves the 2D Schrödinger-Poisson system by means of the finite difference method. It is a robust simulator that the device can be defined as a closed system (two dimensions confined), semi-open system (one dimension confined and one dimension open), and an open system (all dimensions open); it also has models for ballistic current. Then, another complete work was the one developed by **Polizzi and Abdallah** [34]. The authors propose a methodology for solving in 1D and 2D the Schrödinger-Poisson system, considering either an open or a closed system. In such a work, the device is subdivided in slices of one dimension and the waves functions are calculated in each slice; at the end of the process, the waves functions are integrated to compute the global quantities, i.e., the charge density. This methodology solves the equations by means of the finite element method. Finally, there is another research group from the Technical University of Vienna, which has developed a simulator called Vienna Schrödinger Poisson Solver (**VSP Solver**) [37, 40, 46]. The VSP Solver is a robust and complete semiconductor device simulator with more than twenty models to choice, having particularly a special module that can solve the Schrödinger-Poisson system (1D and 2D) for both closed and open systems. The simulator is based on the volume finite method and allows the definition of a variety of structure devices and a wide variety for materials. Table 2.1 shows a review of gate tunneling simulation methodologies for nano-scaled MOS-FETs.

Author	Year	1D	2D	3D	Model	Method
Harrison [16]	1961	✓			WKB	
Tsu and Esaki [17]	1973	✓			WKB	
Rana [20]	1997	✓			S-P	FDM
Lo, Buchanan y Taur [22]	1997	✓			S-P	
Janik y Majkusiak [25]	1998	✓			Analytic	
Shih et al. [26]	1998	✓			WKB	FDM
Register et al. [27]	1999	✓			WKB	
Mudanai et al. [28]	2000	✓			S-P	FDM
Cai et al. [29]	2001	✓			WKB	
Lee et al. [30]	2002	✓			Analytic	
Spinelli,Pirovano y Lacaita [31]	2002		✓		S-P	FEM
Curatola y Iannaccone [32]	2003		✓		S-P	FDM
Curatola,Fiori y Iannaccone [33]	2004		✓		S-P	FDM
Polizzi y Abdallah [34]	2004		✓	✓	S-P	FEM
Driskill [35]	2004	✓			S-P	FDM
Gu et al. [36]	2004	✓			Analytic	
Gehring [37]	2004		✓		S-P	FVM
Curatola,Doornbos,Loo et al. [38]	2005		✓		S-P	FDM
Karner,Gehring,Holzer,Pourfath,Selberherr [40]	2007		✓	✓	Green Func.	FVM
Soreé,Magnus,Pourtoisé [42]	2008		✓		Analytic	
Anderson [44]	2009			✓	S-P	FDM-FVM
Baumgartner,Stanojevic,Schanss, et al. [46]	2013		✓	✓	S-P	VFM.

Table 2.1: Comparison of gate tunneling simulation methodologies for nano-scaled MOS-FETs.

So far, all these are pure electrical models, but only a few simulators account for the effect of the magnetic field, some of them allows to analyze the transistor under the influence of an external magnetic field. There are many works like those described in [47–50, 52], which model a MOSFET under the influence of a magnetic field clasically. All these works are based on the drift-difussion model in which magnetic field dependent terms are added for accounting the action of the Lorentz' force on the motion of the carriers. **Popovic et al.** proposed a methodology for calculating the drain current under the influence of a magnetic field. Also

this method is based on the drift-difussion model and uses the finite element method. The authors assumed a lineal source-drain potential over the channel length. **Nathan et al.** also used a drift-difussion model that includes magnetic field terms, but they assumed a constant drain source field over the channel length. They used the finite difference method as a discretization method. **Riccobenne et al.** 's model took into account the hole and electron currents. The authors developed their model in a simulation tool called GENSIM and they used a box integration method for the discretization of the system. **Rodríguez et al.** developed a 2D/3D methodology based on the drift-diffusion approximation, which incorporates magnetic field terms. The authors developed their methodology in the MINIMOS-NT simulation tool and used the finite volume method as discretization scheme. **Yosry et al.**, based on the Rodríguez's work, developed a compact model (empirical model) for calculating the drain current under the influece of a magnetic field, which depends on geometrical properties. All these metioned works calculate the drain current (but not the gate tunneling current) under the influence of a magnetic field. However, in order to model the new nano-scaled MOSFETs, models based in quantum mechanics needs to be accounted for.

Until now, there are few simulators that incorporate electromagnetic effects using quantum models, such is the case of Birner et al. [53]. The simulator created by them is called Nextnano and it allows to simulate quantum wires (2D considering a closed system), under the influence of a magnetic field. Although the simulator can compute the wavefunctions and the charge density under the influence of a magnetic field, but it cannot calculate the gate tunneling current. This simulator also is capable of modeling only the charge transport of a transistor without the presence of a magnetic field.

Another interesting work is the one developed by Sudiarta [57], in this work only the Schödinger equation (not coupled with Poisson equation) is solved under the influence of a magnetic field but considering a closed system. A summary of the methodologies developed for modeling transistors under the influence of a magentic field is shown in table 2.2.

Author	Year	Model	Simulation	Current	Numerical method
Popovíc [47]	1984	Drift-Diffusion	2D	Drain current	FEM
Nathan,Huiser y Baltes [48]	1985	Drift-Diffusion	2D	Drain current	FDM
Riccobene,Bürgler y Baltes [49]	1994	Drift-Diffusion	2D	Drain current	FVM
Lau,Ko,Chan [50]	1995	Drift-Diffusion	2D	Drain current	FDM
Rodríguez R., Gutiérrez, Klima y Selberherr [52]	2004	Drift-Diffusion	2D,3D	Drain current	FVM
Birner,Zibold,Andlauer,..,Trellakis,Vogl [53]	2007	S-P	2D,3D	No	
Sudiarta and Geldart [57],	2007	Schrodinger	2D	No	FDM
Yosry,Fikry,El-henawy,Marzouk [55],	2009	Compact model	2D	Drain current	

Table 2.2: Comparison of methodologies for modeling MOSFETs under the influence of a magnetic field.

2.4 Discussion

In spite of the advantages and disadvantages that exhibit the device simulators mentioned above, until now there is no simulation tool that allows to analyze the gate tunneling current of a nano-scaled MOSFET under the influence of a magnetic field. As we mentioned in chapter one, with the emergence of the new electromagnetic characterization techniques, there is a necesity to incorporate thermo-magnetic effects in simulation tools that help us to analyze non uniform conductive properties in nano-scaled MOSFETs.

Taking into account all these properties, in this thesis, in colaboration with the Technical University of Vienna, a simulation methodology for solving the 2D Schrödinger-Poisson system that incorporates the magnetic field and allows to calculate the gate tunneling current of a nano-scaled MOSFET is developed.

In the next chapter the methodology simulation proposed in this work is described.

Chapter 3

Simulation methodology

3.1   Schrödinger-Poisson system

In nano-scaled MOSFETs various quantum effects become dominant over the device perfor-
mance. For instance, gate-oxide tunneling and channel energy quantization are some quan-
tum mechanical effects that impact the MOSFET performance. Calculation of these quantum
effects in nano-scaled transistors are frequently based on the self consistent Schrödinger-
Poisson system. [13]- [46].

The wavefunctions and the energies of the system are calculated by solving the time-
independent Schrödinger equation,

$$\left[\frac{\vec{\hat{p}}^2}{2m^*} + V(\vec{r}) \right] \psi(\vec{r}) = E\psi(\vec{r}),$$

(3.1)

where $\vec{\hat{p}} = -i\hbar\nabla$ is the momentum operator, ψ is the wavefunction, E is the energy
eigenvalue, $V(\vec{r})$ is the potential energy and m^* is the effective mass. The potential $V(\vec{r})$ is
defined by

$$V(\vec{r}) = -q\phi(\vec{r}) + \triangle E_{c_{\vec{r}}}$$

(3.2)

where $\triangle E_{c_{\vec{r}}}$ is the energy potential profile generated by the bending of the oxide-substrate energy bands, q is the electron charge and ϕ is the electrostatic potential.

The relation between the space charge and the electrostatic potential is calculated by means of Poisson equation,

$$\nabla^2 \phi(\vec{r}) = -\frac{q}{\varepsilon} \left(N_d(\vec{r}) - n(\vec{r}) \right), \tag{3.3}$$

where ϵ is the permittivity, ϕ is the electrostatic potential, $N_d(\vec{r})$ is the ionized donor concentration and $n(\vec{r})$ is the electron density distribution. The electron density $n(\vec{r})$ is determined from the solution of the Schrödinger equation and it is given by,

$$n(\vec{r}) = \frac{m^* kT}{2\pi\hbar^2} \sum_i | \psi_i(\vec{r}) |^2 \, ln \left(1 + exp(\frac{E_f - E_i}{kT}) \right), \tag{3.4}$$

where k is the Boltzmann constant, T is the temperature, $\hbar$ is the reduced Planck constant, E_f is the fermi level and E_i is the energy level associated to eigenfunction $\psi_i(\vec{r})$. In equation 3.4, the Fermi-Dirac distribution is assumed. This means, that all the particles into a system are considered identical with half-integer spin. Moreover, the Fermi-Dirac distribution allows to consider the many-particle system in terms of a single particle energy states, in which a null interaction between the particles of the system is considered.

A complete description of the charge transport of a nano-scaled MOSFET can be achieved by means of the self consistent solution of the Schrödinger and Poisson coupled equations. The Schrödinger-Poisson system is solved in a consistent way in order to find the potential distribution and the corresponding carrier concentration. The consistent solution of the system is found by solving both equations in a loop until the solution converges. Figure 3.1 shows the flowchart of the Schrödinger-Poisson system solution.
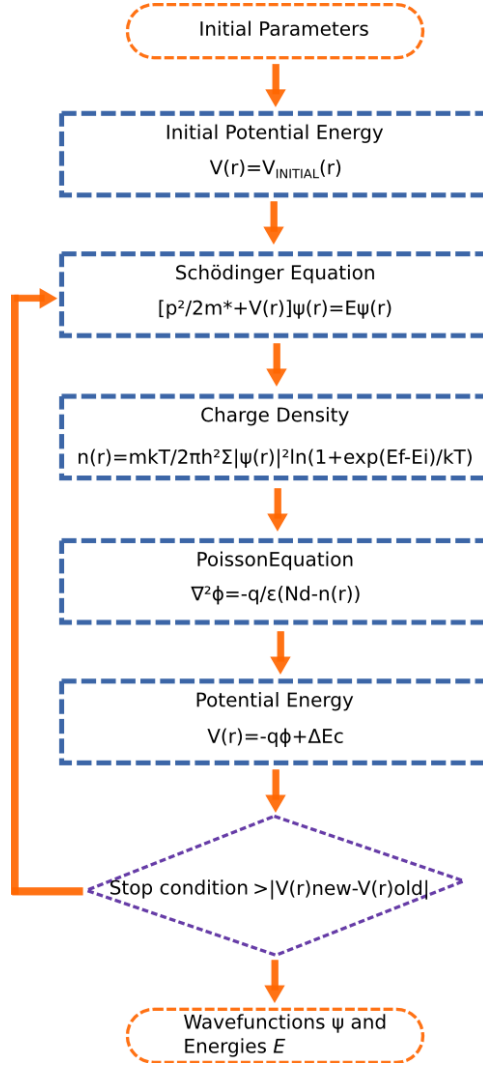
Figure 3.1: Self consistent solution flow chart of the Schrödinger-Poisson system.

3.2 Schrödinger-Poisson system for a constant magnetic field

In the presence of a constant magnetic field $\vec{B}$, where $\vec{B}$ can be described by a vector potential $\vec{A}$ such that

$$\vec{B} = \nabla \times A(\vec{r}), \tag{3.5}$$

the kinetic potential term in the Hamiltonian operator is modified [56]. The quantum mechanical momentum operator $\hat{\vec{p}}$ becomes $\hat{\vec{p}} - q\vec{A}(\vec{r})$ and the Schrödinger equation for a particle in a magnetic field can be defined as

$$\left[\frac{1}{2m^*} (\hat{\vec{p}} - q\vec{A})^2 + V(\vec{r}) \right] \psi(\vec{r}) = E\psi(\vec{r}). \tag{3.6}$$

Suppose we have a surface formed by the xy plane and a constant magnetic field along the z direction is applied (Figure 3.2), then a posible choice for $\vec{A}$ is given by

$$\vec{A} = (0, Bx, 0) \tag{3.7}$$
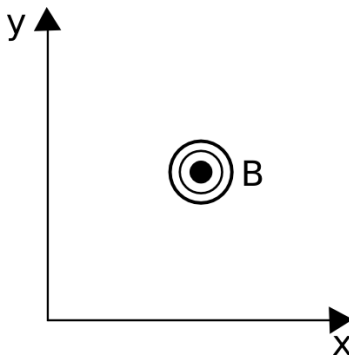
Figure 3.2: Constant magnetic field applied perpendicular to the surface of the xy plane.

Any gradient of a scalar potential $\theta(\vec{r})$ can be added to $\vec{A}$ without changing the value of the magnetic field $\vec{B}$, since $\nabla \times \nabla\theta(\vec{r})$.

This invariance of the magnetic field for different choices of $\theta(\vec{r})$ is called gauge invariance. Another choice for a vector potential $\vec{A}$ that generates the same constant magnetic field $\vec{B}$ along the z-direction is given by

$$\vec{A}(\vec{r}) = (-By, 0, 0) \tag{3.8}$$

In order to incorporate the magnetic field into the Schrödinger equation we modified the general scheme of the solution of the self-consistent loop shown in figure 3.1. The module correponding to the solution of the Schrödinger equation was changed for the Schrödinger equation that includes the magnetic field; see equation 3.6. The proposed scheme of the self-consistent loop that includes the magnetic field is shown in figure 3.3.
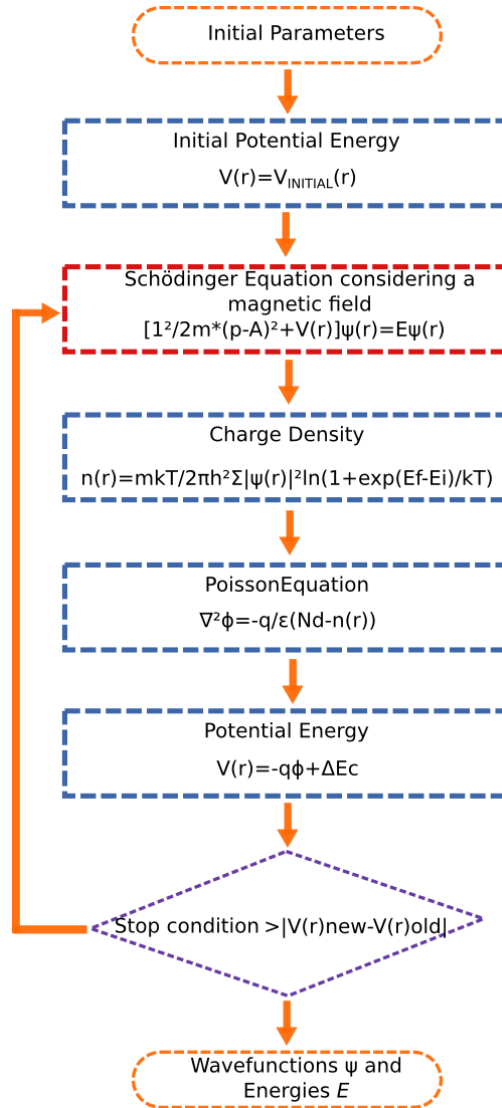
Figure 3.3: Self consistent solution flow chart of the Schrödinger-Poisson system, considering a magnetic field.

3.3 Gate tunneling current

Once the wavefunctions ψ and the energies E are computed, the direct tunneling current can be calculated. The direct tunneling current can be described by the Tsu-Esaki formula [17],

$$J = \int_{E_{min}}^{E_{max}} TC(E_x)S(E_x)dE_x, \tag{3.9}$$

where S represents the supply function, TC represents the transmission coefficient, E_x represents the electron kinetic energy, E_{min} represents the lower energy and E_{max} represents the higher value of the discretized energies into the potential well. The supply function is given by

$$S = ln\left(\frac{1 + exp\left[E_{fs} - E/k_BT\right]}{1 + exp\left[E_{fg} - E/k_BT\right]}\right), \tag{3.10}$$

where E_{fg} and E_{fs} are the electron Fermi levels in the gate and semiconductor, respectively, E_x is the electron energy. Moreover, the supply function represents the number of electrons in an energy level, which are available for tunneling through the barrier potential [18].

The transmission coefficient TC represents the probability of a particle tunneling through the barrier potential and it can be calculated as

$$TC = \frac{J_t}{J_i}, \tag{3.11}$$

where the J_t term corresponds to the transmitted current density and J_i corresponds to the incident current density. The current density probability J can be defined as

$$J(\vec{r}) = \frac{q}{2m^*}\left(\psi^*(\vec{\hat{p}}\psi) - (\vec{\hat{p}}\psi)^*\psi\right). \tag{3.12}$$

The simulation methodology proposed in this thesis, for calculating the gate tunneling current under the influence of a magnetic field, is shown in Figure 3.4.
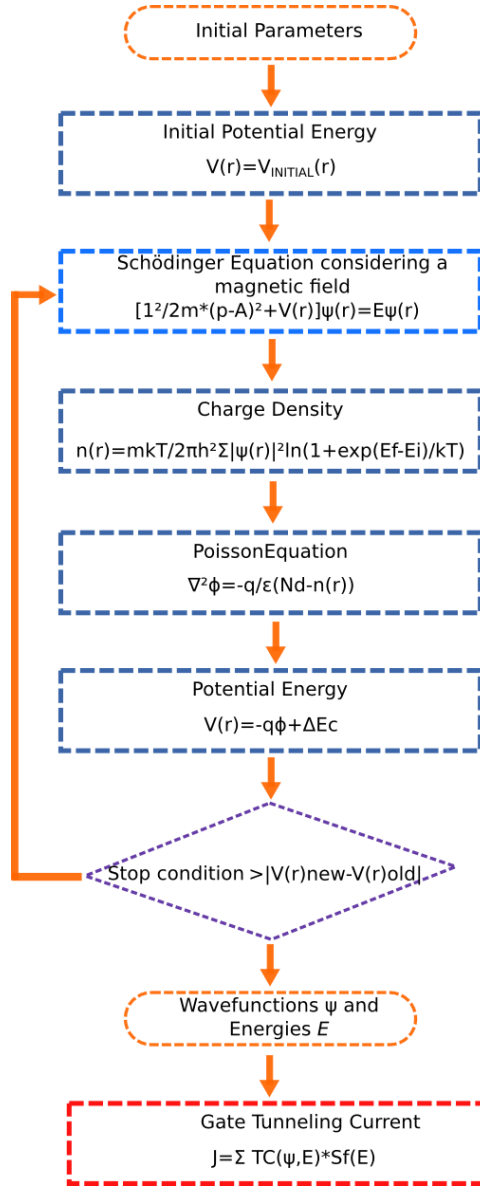
Figure 3.4: Proposed simulation methodology for calculating the gate tunneling current of a nano-scaled MOSFET under the influence of a magnetic field.

3.4 GTS Framework

The Technical University of Vienna in colaboration with Global TCAD Solution Company (http://www.globaltcad.com/en/products/gts-framework.html) have developed a TCAD Framework which includes simulation tools for analyzing 2D/3D semiconductor device structures [60]. The TCAD tool is called GTS Framework and it consists in four simulation tools: GTS Structure, GTS Vision, MINIMOS-NT and VSP tool, Figure 3.5 and Figure 3.6.
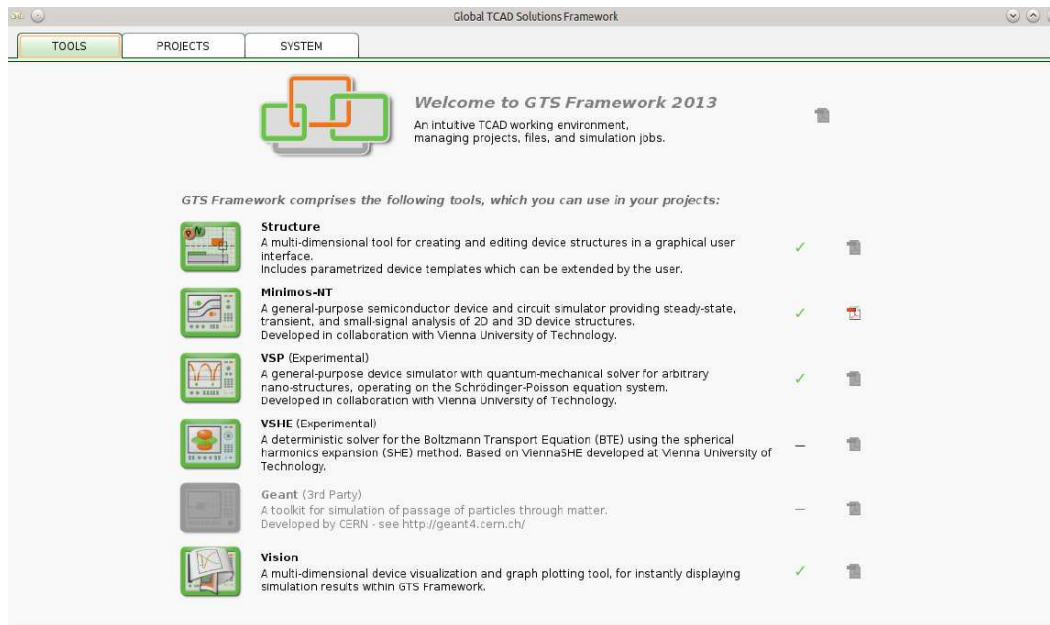
Figure 3.5: Main screen of the GTS Framework.

- **GTS Structure**. This is a graphical simulation tool for definition of 2D/3D semiconductor device structures. With this tool, the meshing, the doping, and the geometry of the device structure can be defined.

- **GTS Vision**. This is a visualization tool, which allows to analyze device structures and simulation results.

- **MINIMOS-NT**. This is a simulation tool for 2D/3D classical modelling of micro-scaled semiconductor device structures.

- **VSP**. The Vienna Schrödinger Poisson (VSP) is a simulation tool for 2D/3D quantum modelling of nano-scaled semiconductor device structures [65–67].

(a) GTS Structure.

(b) GTS Vision.

(c) MINIMOS-NT.

(d) VSP.
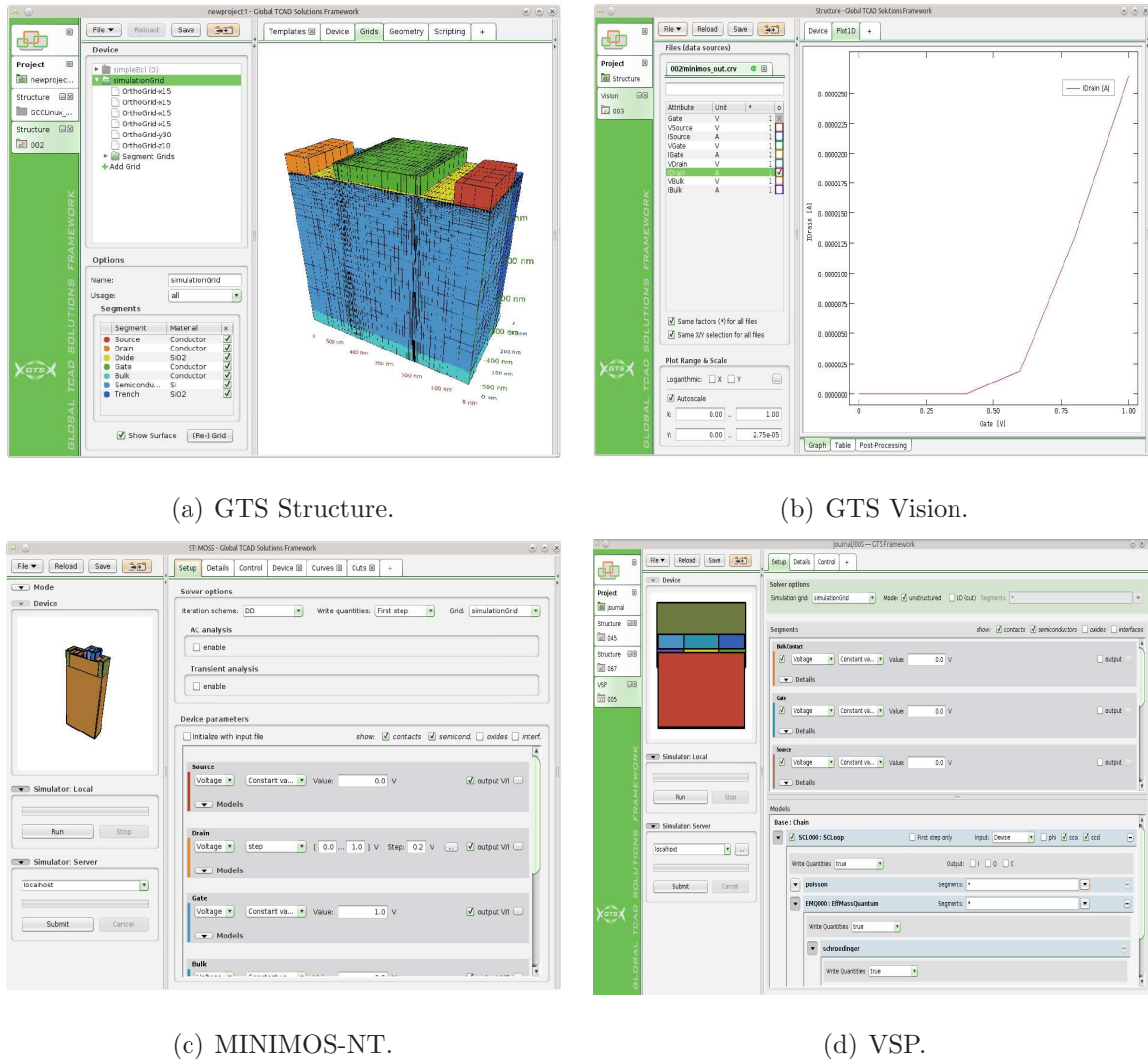
Figure 3.6: Simulation tools inside GTS Framework

3.4.1 Vienna Schrödinger Poisson solver VSP

The VSP simulation tool is focused in the solution of the Schrödinger-Poisson equations system. The VSP is developed in C++ programming language under the object oriented paradigm and it uses stable libraries (Blas, Lapack and Arpack) for numerical calculations.

The flowchart of the VSP module is shown in Figure 3.7. The VSP requires two input files: the semiconductor device structure created in the GTS Structure tool (Figure 3.8(a)) and the ipd file in which the initial conditions and models are defined (Figure 3.8(b)).
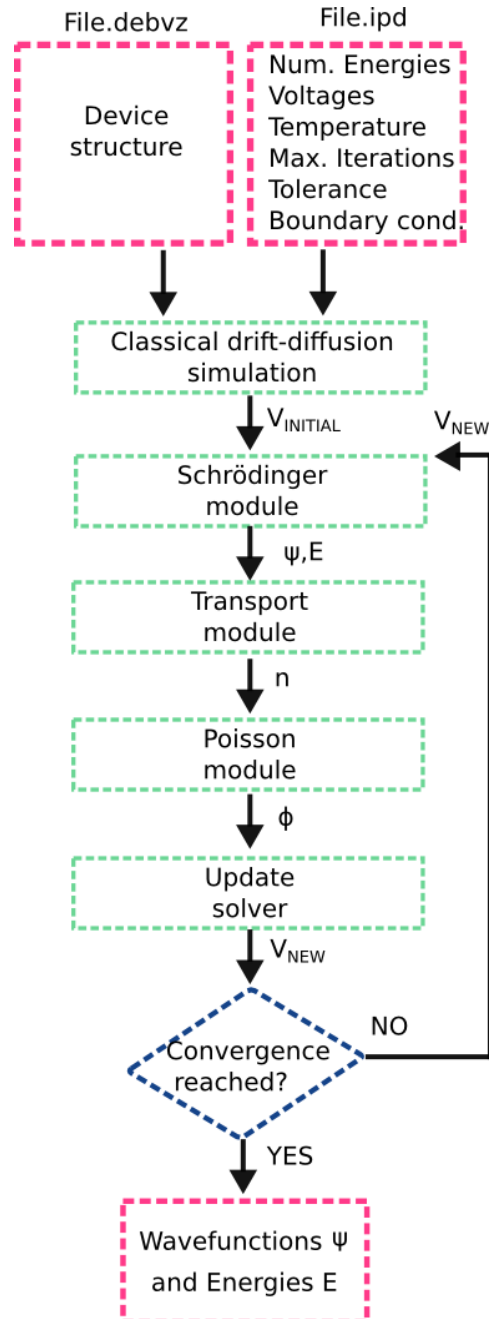
Figure 3.7: Flowchart of the VSP solver.

Once the initial parameters are established, the initial guess value for the potential energy
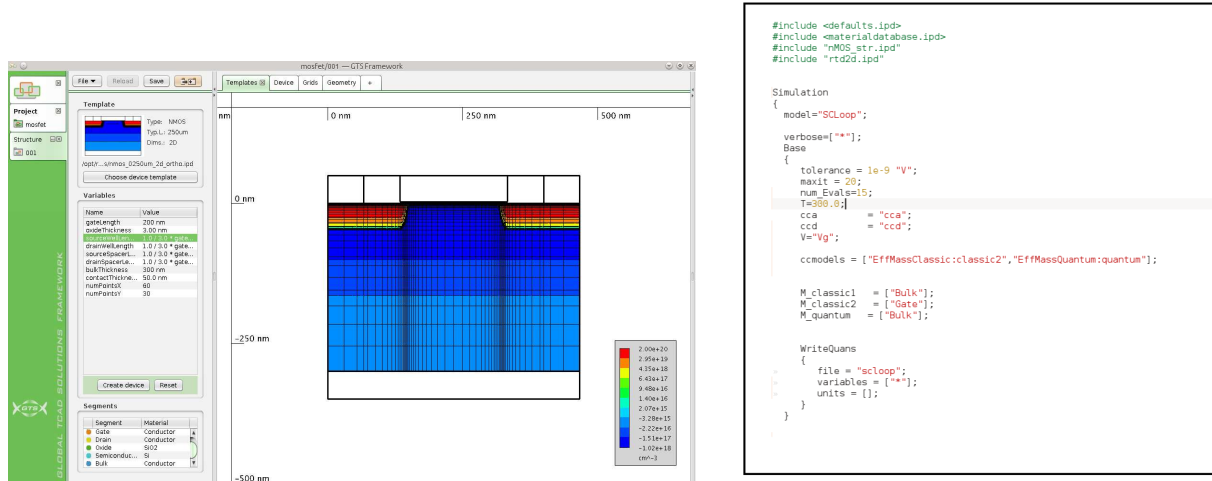
(a) Structure device.

(b) File.ipd.

Figure 3.8: Input files of VSP tool.

$V_{INITIAL}$ is calculated by means of a clasical model simulation (drift-diffusion model). This potential energy $V_{INITIAL}$ is used in the first iteration of the Schrödinger equation and by means of the Finite Volume Method [63], and the ARPACK numerical library [64], the wavefunctions and energies are calculated. Then, the wavefunctions and energies obtained from the Schrödinger module are used in order to calculate the charge density, which then it is used in the Poisson module to obtain the electrostatic potential ϕ. Using the electrostatic potential ϕ a new potential energy is calculated. If the difference between the new potential energy and the old potential energy is less than a convergence criterion, the iteration loop stops. Otherwise, the new potential energy V_{new} is used in the Schrödinger equation and the process is repeated until the convergence criterion is reached.

The output of the VSP module are the wavefunctions and the discretized energies which are saved in a .debvz file, see Figure 3.9.

The VSP procedure to solve numerically the differential equations into the Schrödinger-Poisson system is defined by three stages: definition of the boundary conditions, conversion of the differential equations into a system of algebraic equations, and finally the solution of the algebraic equations, see Figure 3.10.
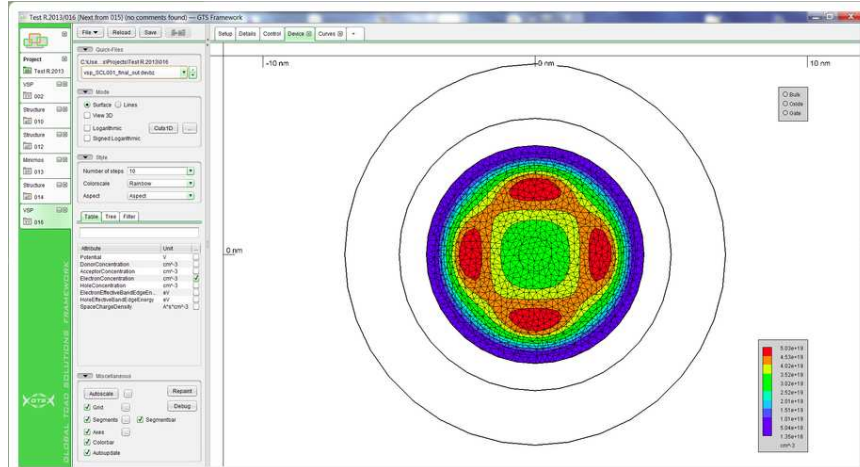
Figure 3.9: Wavefunction of a cross section of a circular nanowire.

- **Definition of the boundary conditions**. The VSP uses closed boundary conditions, which means that the wavefunctions vanish to zero at the $Si - SiO_2$ interface. These boundary conditions do not allow that the wavefunctions pass through the barrier potential, thus the tunneling current cannot be calculated.

- **Discretization of differential equations**. The VSP tool uses the finite volume method as a discretization method. The finite volume method (FVM) is a method to approximate the solution of a partial differential equation [61–63]. The FVM uses the representation of the partial differential equation (3.13) by its integral form as is show in equations 3.14 and 3.15.

$$u_{xx}(x) = f(x) \tag{3.13}$$

$$\int_{x_i-1/2}^{x_i+1/2} u_{xx}(x)\, dx = \int_{x_i-1/2}^{x_i+1/2} f(x)\, dx \tag{3.14}$$

$$u_x(x_{i+1/2}) - u_x(x_{i-1/2}) = \int_{x_i-1/2}^{x_i+1/2} f(x)\, dx). \tag{3.15}$$

The FVM takes into account three points in the mesh $x_{i-1/2}$, x_i, $x_{i-1/2}$, and with this information the derivative can be approximated, see Figure 3.11.

Figure 3.10: Flowchart of the VSP procedure to solve numerically a partial differential equation.

Figure 3.11: Discretization points using finite volume method.

Then by means of the midpoint integration rule [61, 62],

$$\int_{x_0}^{x_1} f(x)\,dx \approx MP(f, h) = hf(x_0 + \frac{h}{2}), \tag{3.16}$$

the right-hand side of equation 3.15 can be approximated by,

$$\int_{x_i-1/2}^{x_i+1/2} f(x)\,dx \approx h f(x_i),$$ (3.17)

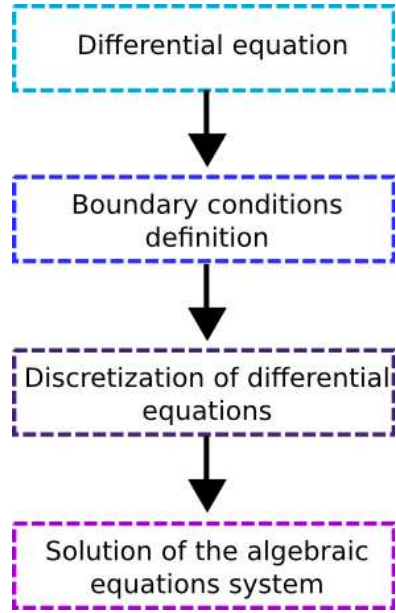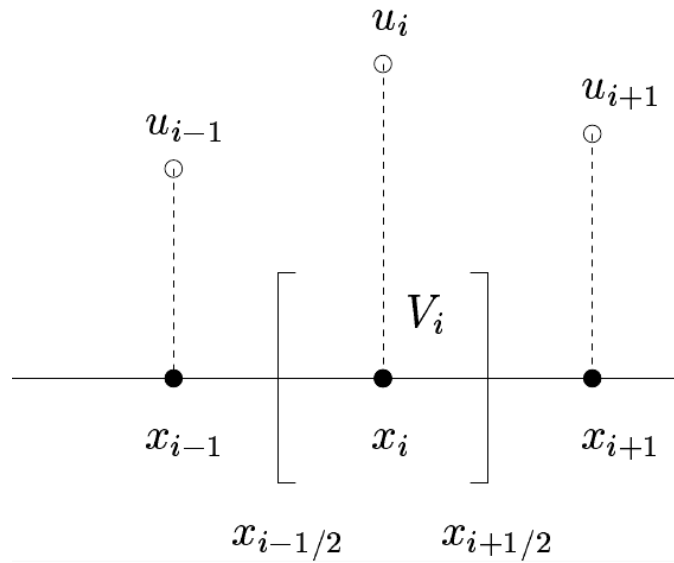and the left-hand side can be approximated by central finite differences by

$$u_x(x_{i+1/2}) - u_x(x_{i-1/2}) \approx \frac{u(x_{i+1}) - u(x_i)}{h} - \frac{u(x_i) - u(x_{i-1})}{h}.$$ (3.18)

Finally the discretized equations are defined as

$$u(x_{i+1}) - 2u(x_i) + u(x_{i-1}) = h^2 f(x_i)$$ (3.19)

- **Solution of the algebraic equations**. After differential equations are dicretized, the set of algebraic equations are solved for each node in the mesh. The system is solved by means of general solution methods (Gauss-Jordan, LU descomposition, Gauss-Seidel). Particularly, the VSP tool uses the ARPACK numerical library to solve the algebraic system [64].

3.5 Computer implementation of the proposed simulation methodology into the VSP tool

The Vienna Schödinger-Poisson tool does not consider magnetic effects on the Schödinger-Poisson coupled equations system. Moreover, the VSP neither allows to calculate tunneling currents because it considers only closed boundary conditions. In this thesis, we made a colaboration with the Technical University of Vienna and we added a module for calculating the gate tunneling current under the influence of a magnetic field.

The first step in order to incorporate the magnetic field was to define the magnetic vector potential $\vec{A}$. Because in this tesis, we are interested in analyzing the magnetic effects on the gate tunneling current, the magnetic field $\vec{B}$ was applied parallel to the surface of the MOSFET and perpendicular to the gate current lines (Figure 3.12).

Thus, we defined the vector potential $\vec{A}$ such as

$$\vec{A}(\vec{r}) = -y\vec{e_x}B,$$ (3.20)
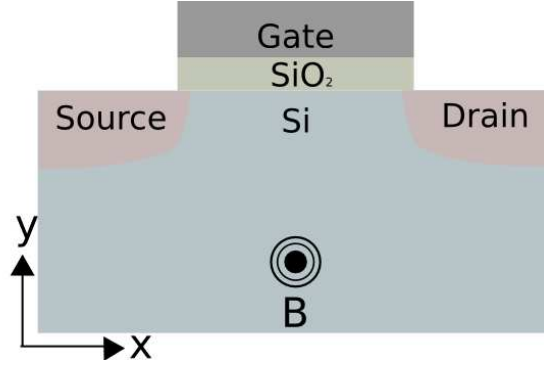
Figure 3.12: magnetic field B was applied parallel to the surface of the MOSFET and perpendicular to the gate current lines.

where $\vec{e_x}$ is the cartesian unit vector along the z-direction and $\vec{B}$ is the component of magnetic field, in the z-direction.

Moreover, we had to change the Schödinger equation by adding the vector potential A in the kinetic energy term as is described in equation 3.6. The VSP solves the Schrödinger-Poisson system considering a closed system. A closed system means that all axes are confined and at the boundaries of the device geometry the wavefunctions vanish 3.13.

Figure 3.13: System with closed boundary conditions in which the wavefunctions are transmitted and reflected.

In order to calculate the gate tunneling current in a nano-scaled MOSFET, open boundaries need to be considered. The energies of an open system are complex values $E = E_r + Ei$

where the real part E_r is the resonant energy and the imaginary part E_i can be understood as the decay probability of the electron can have into the domain. In recent works, a method based on absorbing boundary conditions (Perfectly Matched Layer method) has been applied to determine the energies of an open system [40, 73, 74]. The PML method adds absorbing layers with non physical meaning which act as artificial open boundary conditions preventing reflections 3.14. When the wavefunction enters to the absorbing layer, the wavefunction is attenuated and it decays exponentially.

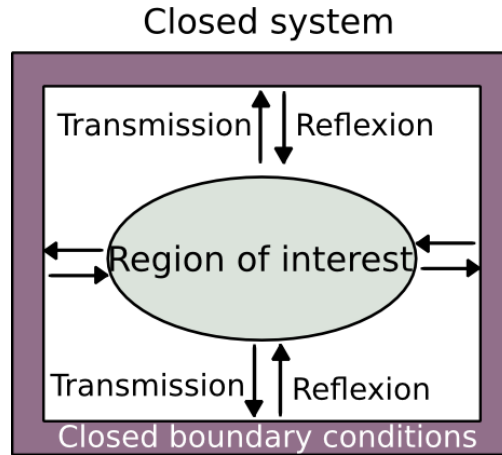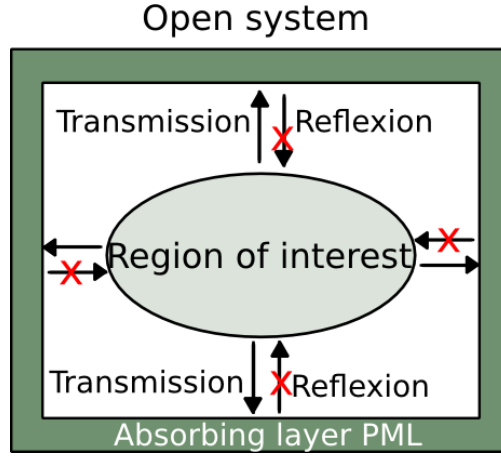Figure 3.14: System with open boundary conditions by adding absorbing layers in which the wavefunctions are transmitted but not reflected.

This process is done by means of replacing coordinates x by stretched coordinates $\tilde{x} = x + if(x)$, where $f(x)$ represents how the imaginaty axis has been deformed. Then the derivatives of the system can be expressed as

$$\delta\tilde{x} = \left(1 + i\frac{\delta f(\vec{x})}{\delta x}\right)\delta x, \tag{3.21}$$

There is a variable change in order to define the equation in terms of the real coordinates x where $s(x) = 1 + i\sigma_x(x)$, then the derivatives of the equation are changed by

$$\frac{\delta}{\delta\tilde{x}} = -\frac{1}{s_x}\frac{\delta}{\delta x}, \tag{3.22}$$

In the PML regions where σ is equal to zero, the term s_x is equal to 1 and the wavefunction does not change. For the case when $\sigma > 0$ the imaginary part of the wavefunction increases and as a result the wavefunction decays exponentially. This happens because the wavefunction can be seen as $e^{ikx} = e^{ik(Rex+iImx)} = e^{ikRex-kImx}$, thus the solution exponentially decays as Imx increases (where the equation is evaluated in the positive real and imaginary axis).

Chapter 4

Results and discussion

4.1 Magnetic effects on wavefunctions and energies

As a first benchmark device a circular n-type Si nanowire of 30 nm with equivalent oxide thickness EOT of 2.0 nm, $N_D = 1 \cdot 10^{17}$ cm^{-3} and $N_A = 3 \cdot 10^{17}$ cm^{-3} was used for analyzing the magnetic effects on the wavefunctions and energies. For this experiment, closed boundary conditions were used. Thus, the wavefunctions are confined in the silicon region and they vanish to zero at the $Si - SiO2$ interface. The magnetic field B was applied perpendicular to the xy plane of the nanowire, see Figure 4.1.
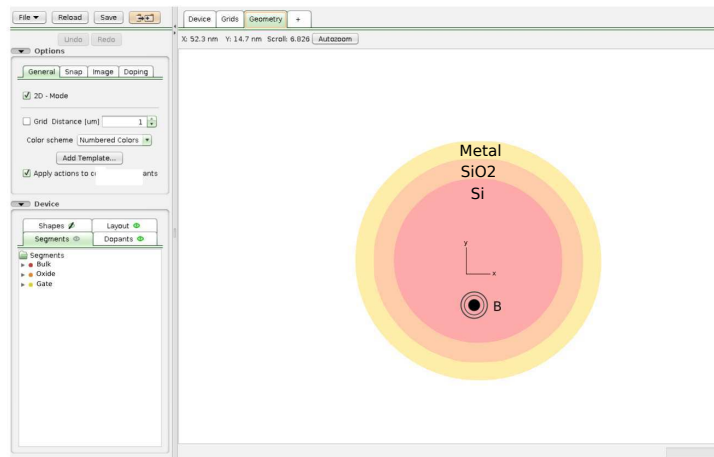
Figure 4.1: Circular nanowire structure

Figures 4.2 and 4.3 show the probability density $|\psi|^2$ of wavefunctions of the second and sixth state respectively, under the influence of a magnetic field B of 0T, 50mT, and 500mT.

When a perpendicular magnetic field is applied, there is a effect called hybridization or mixture of states and the wavefunctions are modified.

This happens because when a magnetic field is applied the Hamiltonian is perturbed and no longer separates the states and them begin to mix.

As a direct consequence the mixing of states results in new hybrid states, which results in an increase of the propability of found electrons where before cannot be found.

The hybridization between two degenerated electronic states produces a repulsion between each other in energy which lifts the degeneracy of the states.

(a) B=0T   (b) B=50mT   (c) B=500mT
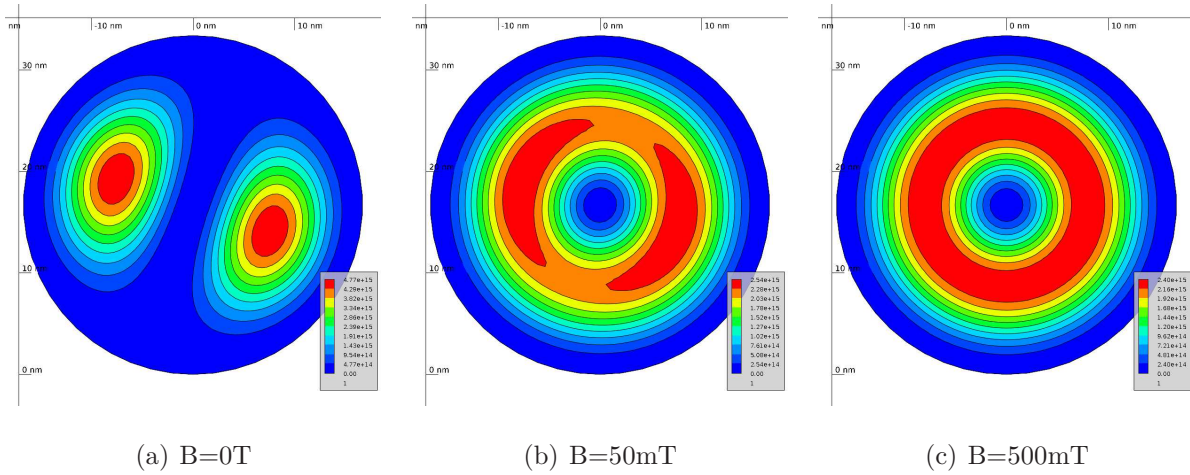
Figure 4.2: Probability density $|\psi|^2$ of the second level wavefunction of a cross section of a circular nanowire under the influence of a magnetic field applied perpendicular to the xy plane.

Moreover, when hybridization between two degenerated electronic states occurs, the states repulse each other in energy resulting in an energy splitting which is called Zeeman effect [71, 72] (Figure 4.4).

(a) B=0T (b) B=50mT (c) B=500mT
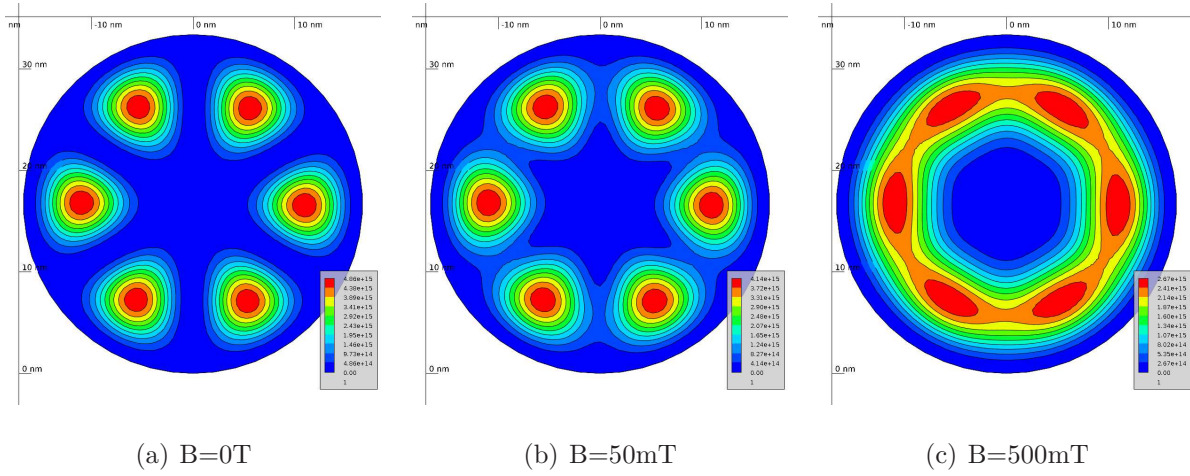
Figure 4.3: Probability density $|\psi|^2$ of the sixth level wavefunction of a cross section of a circular nanowire under the influence of a magnetic field applied perpendicular to the xy plane.
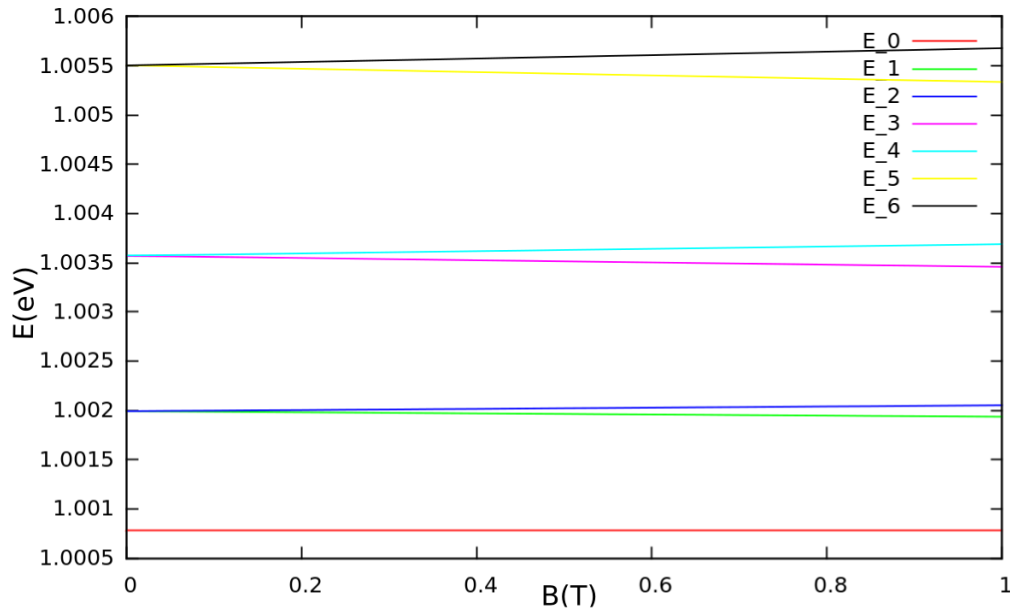
Figure 4.4: Split energies due to the applied magnetic field.

Furthermore, in Figure 4.5 we see the probability density of the second state $|\psi_2|^2$ and the density probability of the third state $|\psi_3|^2$.

37

For this case, both states are degenerated because they have the same energy value. When a perpendicular magnetic field is applied, the second and third states begin to mix and with stronger magnetic fields both states will exhibit a circular or ring shape [72].

(a) ψ_2,B=0T

(b) ψ_3,B=0T

(c) ψ_2,B=500mT

(d) ψ_3,B=500mT
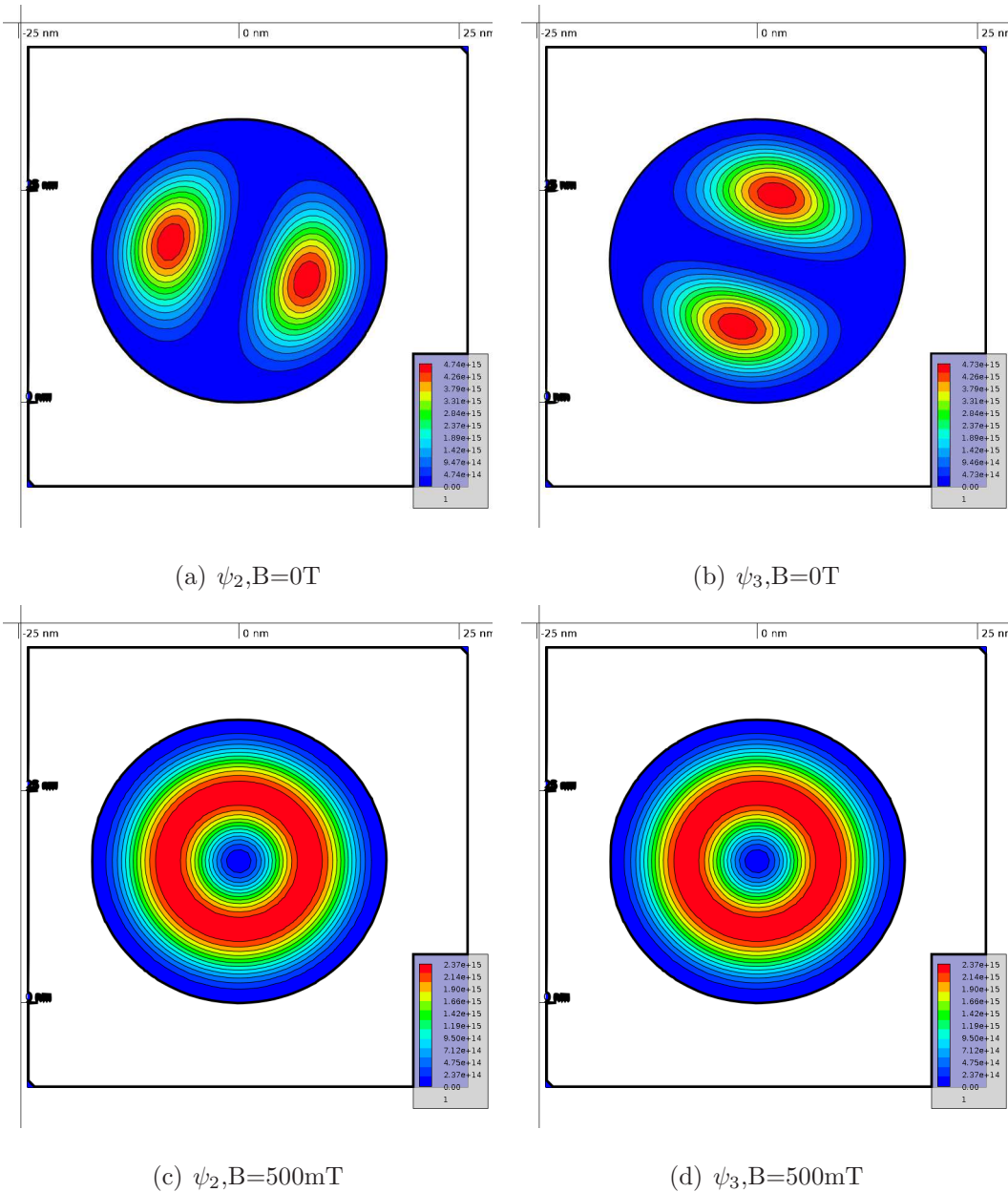
Figure 4.5: Hybridization of ψ_2 and ψ_3 states.

4.2 Magnetic effects on nano-scaled MOSFET

Asymmetrical channel conductivity

In the work's of Póndigo developed at INAOE [6, 68], the $Id - Vg$ characteristic curve of the 28-nm nMOSFET, without applying an external magnetic field, was measured (Figure 4.6). Ideally, the transistor should be off at $Vg = 0.0$V, but we see in Figure 4.6 that there is a leakage current I_{off} of 10pA at $Vd = 0.1$V.

Furthermore, the subthreshold sope S should be close to its ideal 60mV/dec value. The subthreshold slope S is given by

$$S = \left[\frac{\delta V_g}{\delta log(I_d)} \right] = ln(10) \frac{mkT}{q}, \tag{4.1}$$

where k is the Boltzmann constant, q is the electron charge, and m is a numerical factor in the 1 to 2 range.

An external magnetic field was applied perpendicular to the surface of the MOSFET, the leakage current I_{off} the subthreshold slope S were measured as a function of the magnetic field B (Figure 4.7).

We see that there is no parabolic reduction of the I_{off} current and neither in the subthreshold slope S [69]. Under an ideal situation, for negative B field the current lines should be deflected by the Lorentz force to the left side in the x-axis direction, while for positive B field to the right side of the FET channel plane showing a symmetrical behavior, see inset Figure 4.7.

Moreover, they measured the transconductance gm and the threshold voltage Vt as a function of a magnetic field (Figure 4.8). We see that there is an asymmetry in the transconductance and also in the threshold voltage. There is an asymmetry in the experimental results which cannot be explained with the assumption of an isotropic and homogeneous channel FET conductance [5]. This non-homogeneous conductance can be attributed to the
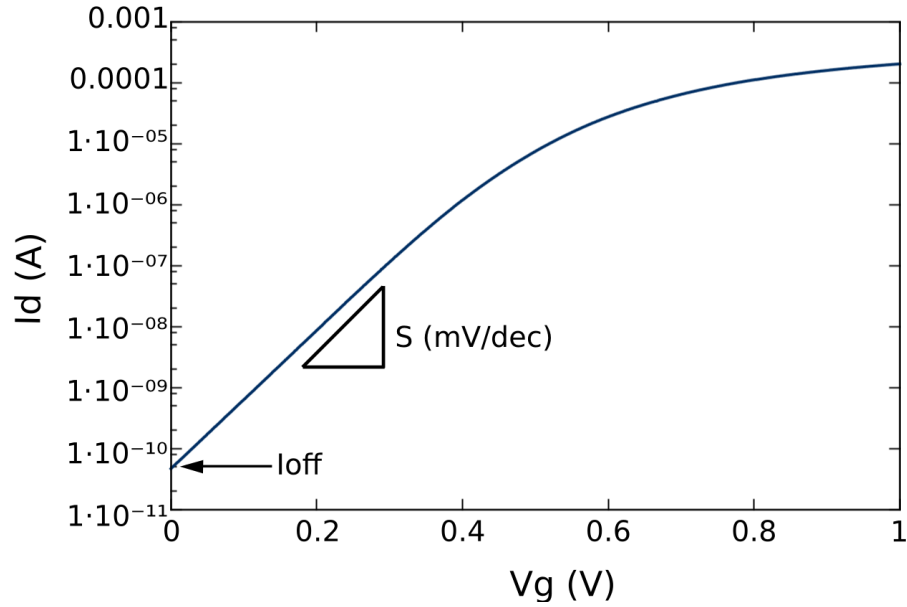
Figure 4.6: Measurement $Id - Vg$ characteristic curve of a 28-nm nMOSFET with $B = 0$mT with $V_{DS} = 0.1$ V.
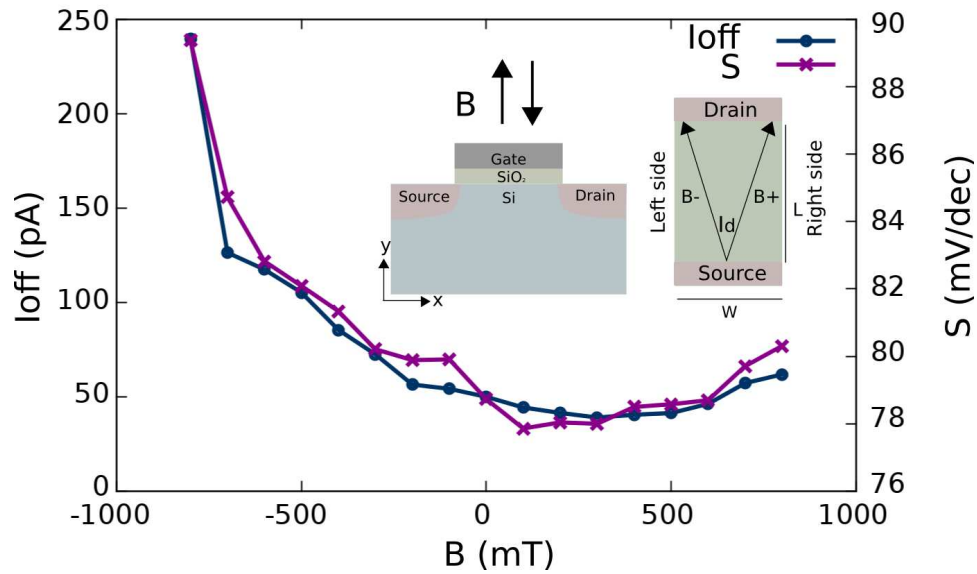
Figure 4.7: Measurement of the leakage current I_{off} and subthreshold slope S for 28-nm nMOSFET as a function of a magnetic field applied perpendicular to the surface of the MOSFET with $V_{DS} = 0.1$ V.
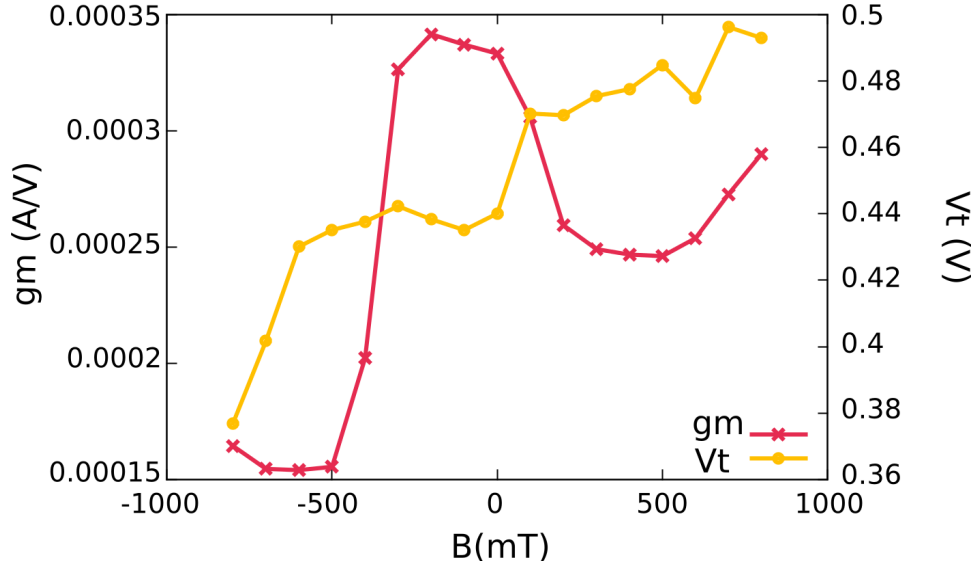
Figure 4.8: Measurement of the transconductance gm and subthreshold voltage Vt for 28-nm nMOSFET as a function of a magnetic field applied perpendicular to the surface of the MOSFET with $V_{DS} = 0.1\,\text{V}$.

asymmetry and non-homogenity caused by the mechanical stress induced in the transistor or by process variations [3].

Magnetic effects on the gate tunneling current

In order to analyze the non-homogenity of the gate tunnel current under the influence of an external magnetic field $\vec{B}$, we used as a benchmark device a 28-nm n-type Si MOSFET with equivalent oxide thickness EOT of 2.0 nm, gate width W of 1.0 μm, $N_D = 5 \cdot 10^{19}$ cm^{-3} and $N_A = 3 \cdot 10^{18}$ cm^{-3}, see Figure 4.9.

We applied an external magnetic field parallel to the surface of the channel (z-axis) and perpendicular to the gate current lines (Figure 4.10). The measurement tunneling current was compared with the results obtained from our simulation tool. Figure 4.10 shows the measured and simulated magnetomodulated gate current $\Delta I_G = I_{G_{B \neq 0}} - I_{G_{B=0}}$ under the influence of a static magnetic field $B = \pm 400$mT with $V_{DS} = 0.5$V. There is a good agreement between measurement data and the results obtained with our simulation tool. The error obtained
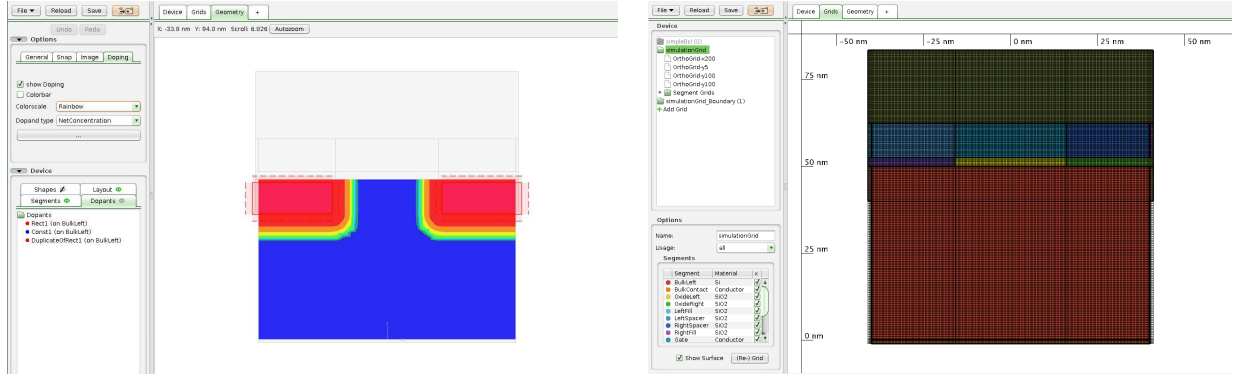
(a) Doping definition

(b) Grid definition

Figure 4.9: Definition of a nano-scaled 28-nm MOSFET into the GTS Strcuture tool.

between simulation and measured data could be associated with the fact that a homogeneous and symmetrical oxide is considered in the simulation settings.
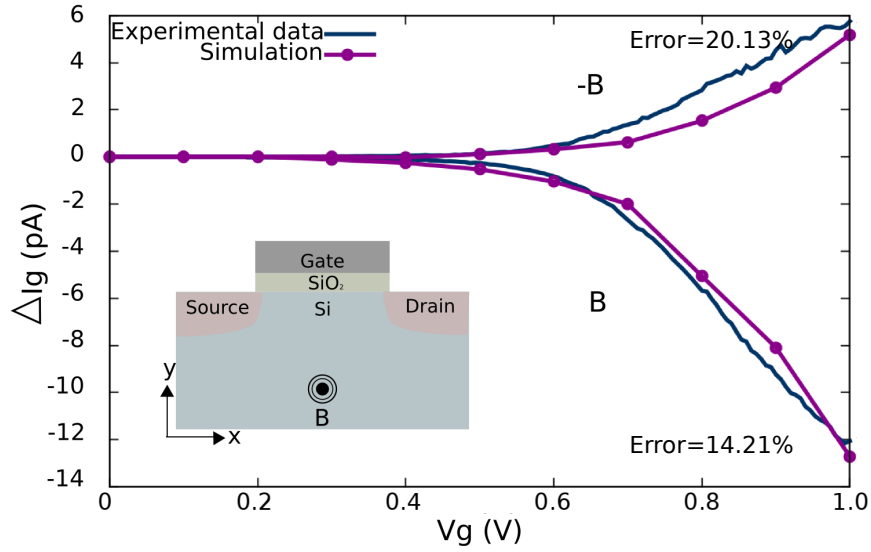
Figure 4.10: Magneto-modulated gate current ΔI_G for 28-nm nMOSFET at $V_{DS} = 0.5\,\text{V}$ in a magnetic field $B = -400\,\text{mT}$.

As we mentioned before, a strained 28-nm MOSFET may have a non uniform conductance along the length and width of the channel [3, 6], such a non-uniformity of the conductive properties of the channel can be recreated by means of a non-uniform gate oxide thickness or by means of a non-uniform doping profile. In this work, we recreate such a non-uniformity for both cases.

Figure 4.11 shows the percentage of change of magnetomodulated gate current ($\Delta I_G/I_G$) for three different non uniform oxide profiles. Oxide number one has $T_{oxL} = 2.0$ nm and $T_{oxR} = 2.5$ nm, oxide number two has $T_{oxL} = 2.0$ nm and $T_{oxR} = 2.6$ nm, and oxide number three has $T_{oxL} = 2.0$ nm and $T_{oxR} = 2.7$ nm. We see that there is a higher percentage of change of ΔI_G for oxide three which is the most non uniform device structure. In Figure 4.12 we show that the asymmetry of $\Delta Ig - B$, with respect of the ΔI_G when $\vec{B} = 0$, increases and tends to saturate at large values for the oxide thickness non-uniformity.

Figure 4.11: Simulated percentage of change of magneto-modulated gate current $\Delta I_G/I_G(\%)$ for 28-nm nMOSFET with $V_{DS} = 0.0\,\text{V}$ and $V_G = 1.0\,\text{V}$.

Moreover, the behavior of the supply function S and the transmission coefficient TC for the third oxide profile under the influence of a magnetic field are shown in Figure 4.13. We see that for high values of the magnetic field B, depending on the magnetic field polarity, the transmission coefficient decreases or increases. This happens due to the non uniformity of the oxide, there is a higher transmission probability when electrons are deflected by the Lorentz force to the thinner oxide side. Moreover, the supply function decreases when a magnetic field is applied. A reduction of the supply function implies a decrease of the charge population with an energy range with a transmission probability to tunnel through the gate oxide. Therefore, a reduction of the supply function implies a reduction of the current that tunnels through the gate oxide.
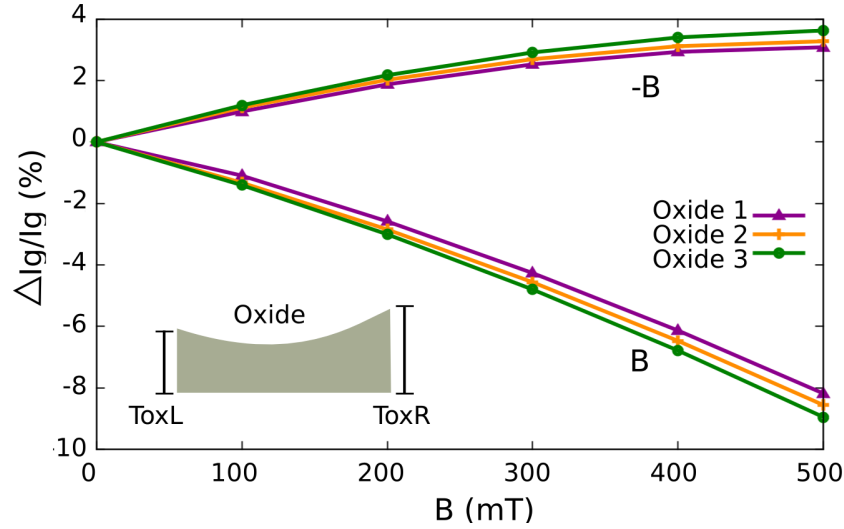
Figure 4.12: Simulated percentage of change of magneto-modulated gate current $\Delta I_G/I_G(\%)$ for 28-nm nMOSFET with an increase in the right side in the x-axis direction (towards the drain side) of the oxide thickness $ToxR$ in a magnetic field $B = -500\text{mT}$.
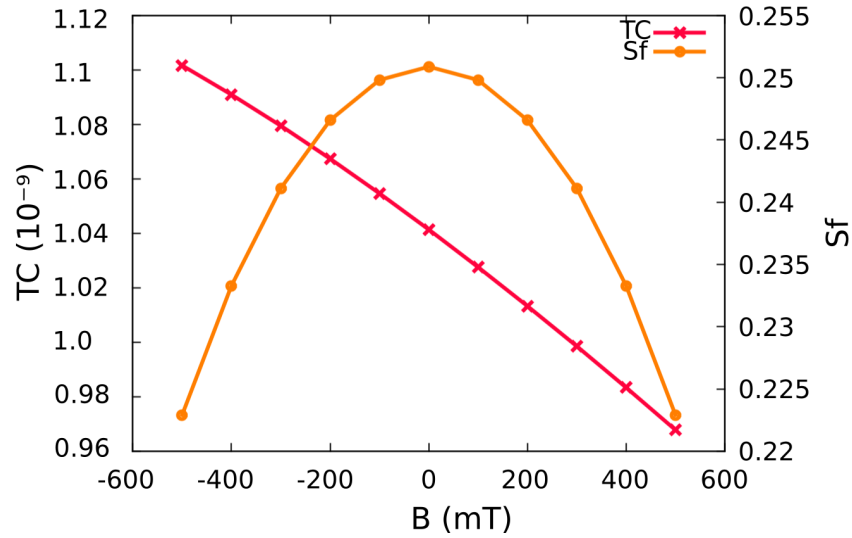
Figure 4.13: Simulated supply function Sf and transmission coefficient TC for oxide number three under the influence of a magnetic field with $V_{DS} = 0.0\,\text{V}$ and $V_G = 1.0\,\text{V}$.

In order to study the effects of a nano-scaled MOSFET having an non homogeneous channel conductive properties, a structure with three different non uniform doping profiles has been used, see Figure 4.14. Doping profile number 1 has $DopL = 2 \cdot 10^{18}$ cm^{-3} and

$DopR = 5 \cdot 10^{18}$ cm^{-3}, doping profile number 2 has $DopL = 1 \cdot 10^{18}$ cm^{-3} and $DopR = 5 \cdot 10^{18}$ cm^{-3}, and doping profile number 3 has $DopL = 9 \cdot 10^{17}$ cm^{-3} and $DopR = 5 \cdot 10^{18}$ cm^{-3}.
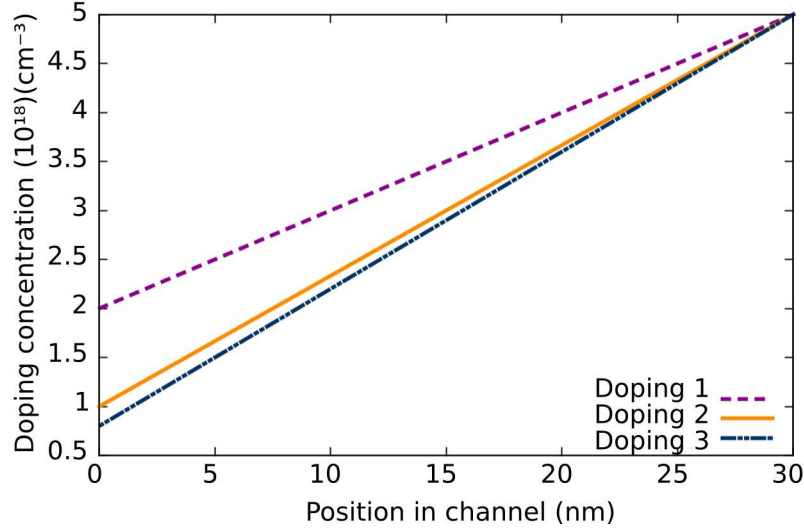
Figure 4.14: Non uniform doping distribution profiles in the channel for 28-nm nMOSFET.

Figure 4.15 shows the percentage of change of magnetomodulated gate current $(\Delta I_G / I_G (\%))$ for the defined non uniform doping profiles.

In Figure 4.15, we see that there is a higher percentage of change of ΔI_G when a magnetic field with positive polarity is applied. With a positive B field the current lines are deflected by the Lorentz force to the right side in the x-axis direction (towards the drain side) where there is a larger doping profile. A larger doping profile implies an increase of the threshold voltage which results in a lower inversion layer charge population. Therefore, the supply function decreases and as a direct consequence the tunneling current decreases. The most non-uniform doping profile number three shows the most pronounced asymmetrical magnetomodulated gate current ΔI_G.

Figure 4.16 shows the relation between the non-uniformity of the semiconductor doping profile $\Delta Doping = DopR - DopL$ and the magnetomodulated gate current ΔI_G. The highest doping profile asymmetry results in the largest asymmetrical magnetomodulated gate current ΔI_G.
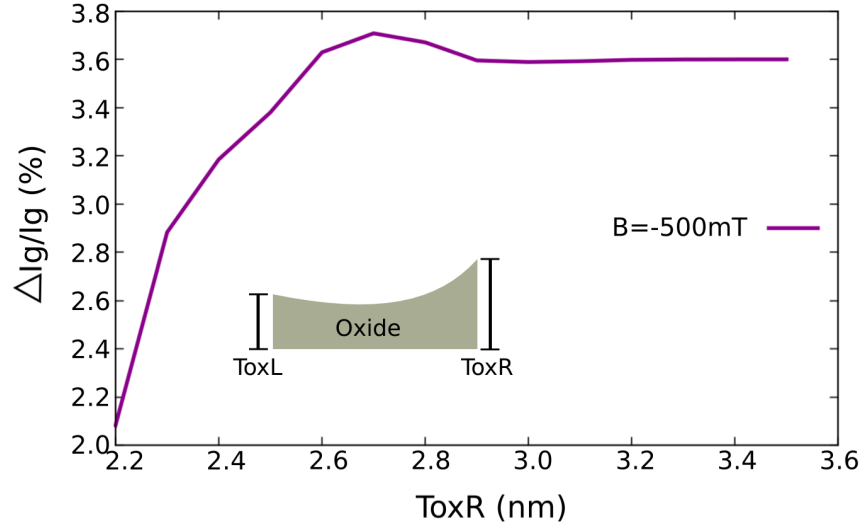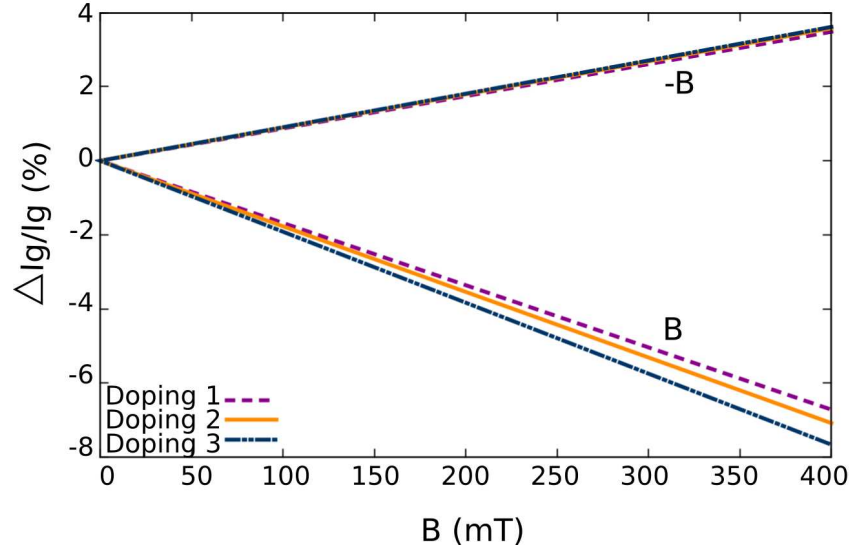
Figure 4.15: Simulated percentage of change of magneto-modulated gate current $\Delta I_G/I_G(\%)$ for 28-nm nMOSFET for three different channel doping profiles in a magnetic field $B = \pm400$mT with $V_{DS} = 0.0$ V and $V_G = 1.0$ V.
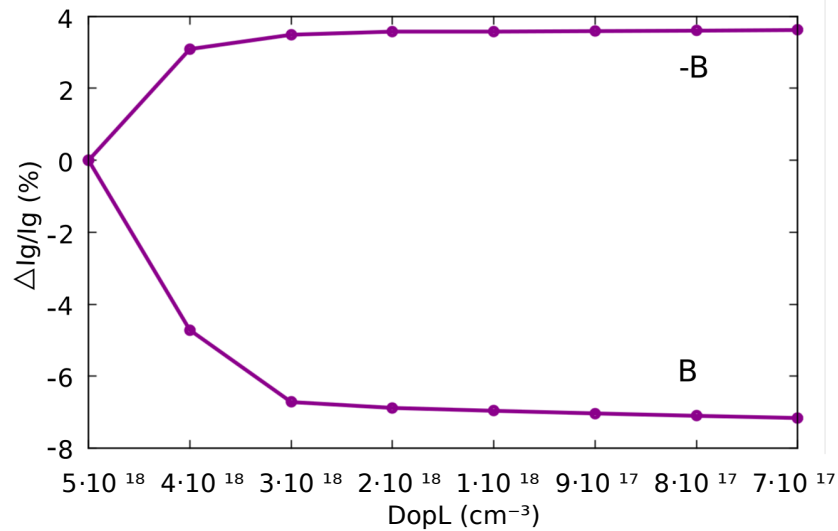
Figure 4.16: Simulated percentage of change of magneto-modulated gate current $\Delta I_G/I_G(\%)$ for 28-nm nMOSFET with channel doping profile variations in a magnetic field $B = \pm400$mT with $V_{DS} = 0.0$ V and $V_G = 1.0$ V.

Thermal effects on the gate tunneling current

In order to study the effects of the temperature on the gate tunneling current of a nano-scaled MOSFET, Figure 4.17 shows the relation between temperature and gate tunneling current

I_G from simulated and experimental data. Moreover, Figure 4.18 shows the same relation $Ig - Temp$ in logarithmic scaled. For this experiment, we used a as a benchmark device a 28-nm n-type Si MOSFET with equivalent uniform oxide thickness EOT of 2.0 nm, gate width W of 1.0 μm, $N_D = 5 \cdot 10^{19}$ cm^{-3} and $N_A = 3 \cdot 10^{18}$ cm^{-3}. For the simulation device, we assumed a uniform oxide and a uniform doping profile along the channel device.
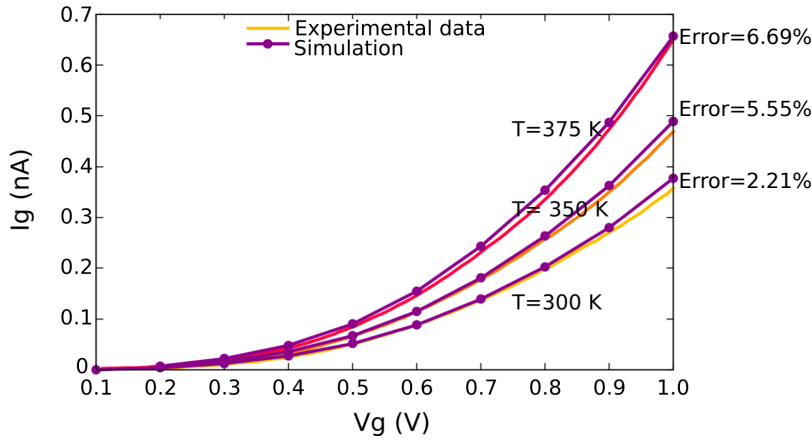
Figure 4.17: Ig-Vg characteristics of 28-nm nMOSFET under the influence of thermal variations at $V_{DS} = 0.5$ V.
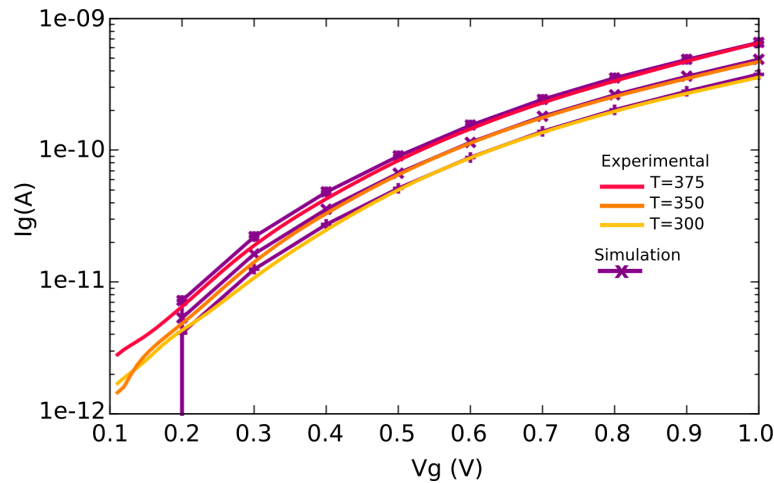
Figure 4.18: Semi-logarithmic Ig-Vg characteristics of 28-nm nMOSFET under the influence of thermal variations at $V_{DS} = 0.5$ V.

There is a good agreement between measurement data and the results obtained with our simulation tool. For the case of $Vg < 0.2$ the simulation tool sets $Ig = 0.0$. Because of that, the error obtained considers only the values of Ig for $Vg >= 0.2V$.

The tunneling current rises as there is an increase in temperature. This happens because temperature affects the behavior of the supply function S and the transmission coefficient TC; see Figure 4.19. With temperature, both the supply function and the transmission coefficient increase [70], and so does the gate tunneling current. For the case of the supply function with more temperature there are more electrons available to tunnel through the barrier potential. While for the case of the transmission coefficient with more temperature the effective mass is changed and there is an increment in the transmission coefficient.
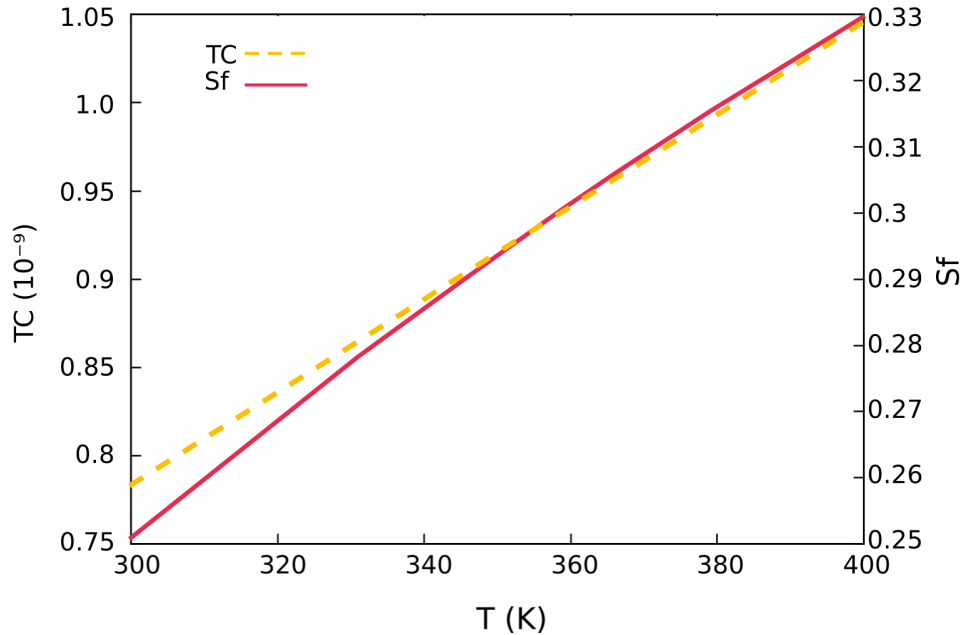
Figure 4.19: Simulated supply function and transmission coefficient of 28-nm nMOSFET under the influence of thermal variations at $V_{DS} = 0.5\,\text{V}$.

Simulation tool performance

In order to analyze the performance of our simulation tool, the runtimes and percentual errors of our methodology were computed. Figure 4.20 shows the runtime of our methodology with

respect to the grid size definition for one voltage step Vg. We see that as it was expected, with a finer grid size the runtime increases. Moreover, we saw that for our particular device size, the device can be divided into a gride size lower than 0.5 nm the potential energy converges.
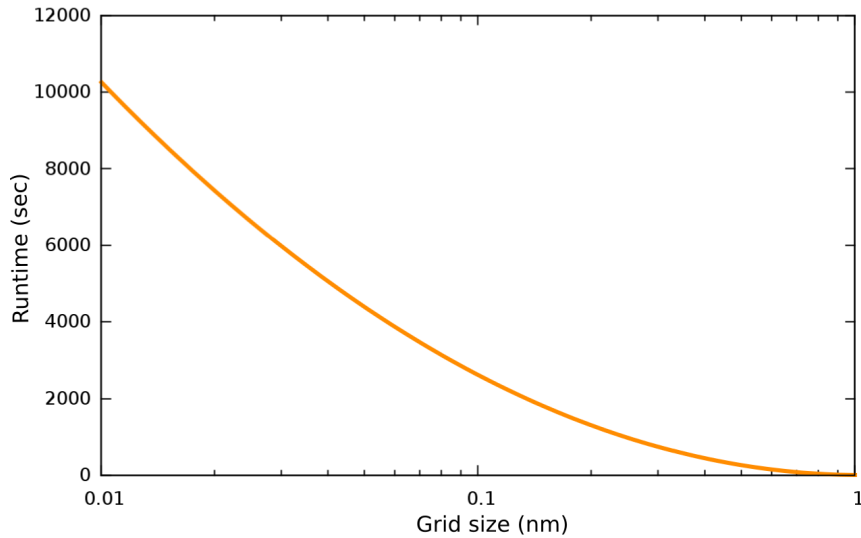
Figure 4.20: Runtime dependence on the grid size definition.

Furthermore, we analyzed the runtime of our methodology with respect to the number of the eigenvalues calculated, see Figure 4.21.It is important to say that only the ten first eigenvalues have a real contribution to the gate current [40].

We also tested the runtime when a magnetic field is applied and we see that there is a difference of 4.453 seconds approximately for considering the magnetic field in our methodology.

The average percentual error between measurement data and simulation results is shown in Figure 4.22. We can see that the maximum error is obtained with a $Vg = 0.2V$ and the minimum error is obtained with a $Vg = 0.7V$.
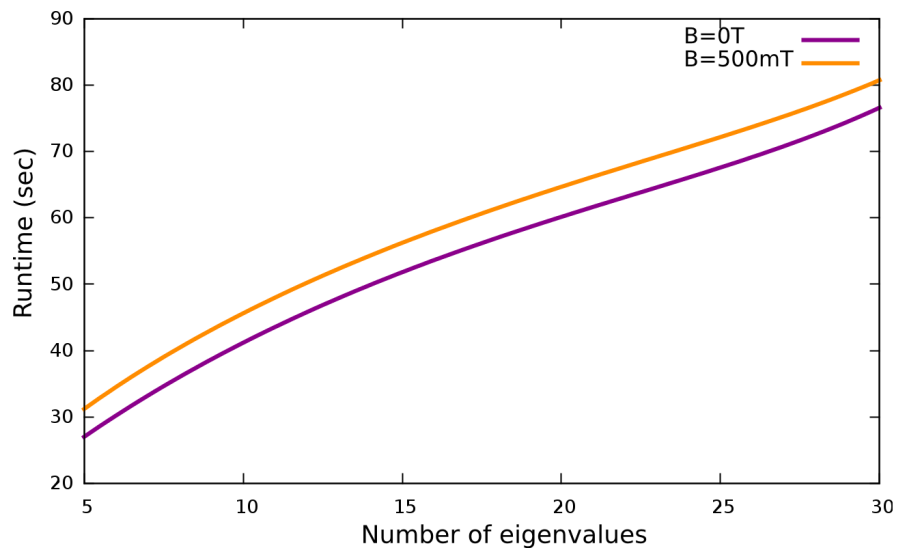
Figure 4.21: Runtime dependence on the number of eigenvalues computed.
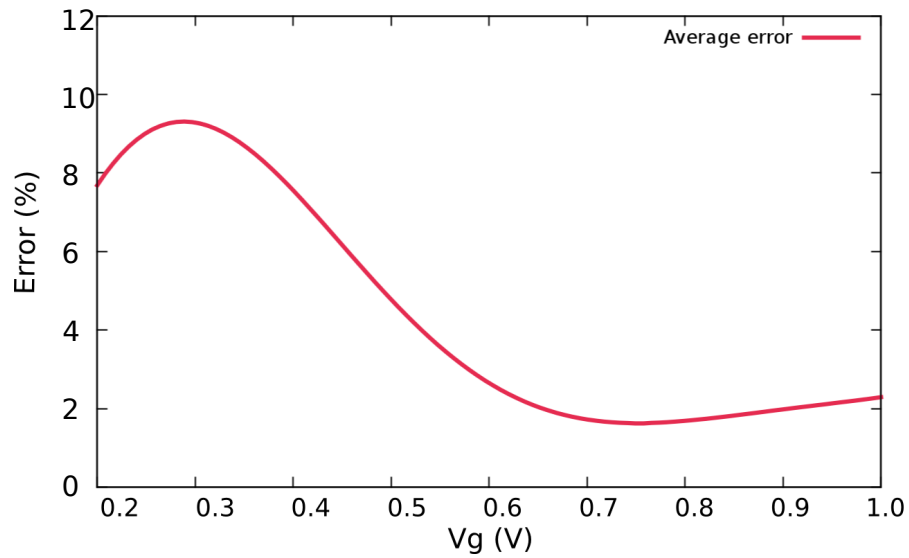
Figure 4.22: Percentual average error simulations.

Chapter 5

Conclusions and future work

A 2D simulation methodology for analyzing thermo-magnetics effects on nano-scaled MOS transistors has been introduced. This has been achieved by incorporating the magnetic field and temperature as additional variables into the solution of the Schrödinger-Poisson coupled system using the Vienna Schrödinger-Poisson solver (VSP) [46]. This implementation into the GTS Framework [60] simulation tool allows us to calculate the gate tunneling current in nano-scaled MOSFET devices under the influence of thermo-magnetics effects.

The calculation of the gate tunneling current has been performed using the Tsu-Esaki model and considering open boundary conditions by using the Perfectly Matched Layer method.

An external magnetic field was applied perpendicular to the gate tunneling current of the MOSFET. With the aplication of the magnetic field, it has been shown a mix of the states of the wavefunctions and the spliting of the energy levels of the system, which have an impact in the gate tunneling current of the MOS device. Moreover, the transmission coeffient and the supply function were calculated in function of the magnetic field and temperature variations.

The non-uniformity of the channel in real strain nMOS devices was reproduced by means of non-uniform oxide profiles and non-uniform doping profiles. By using the magnetic field we were able to scan the non-uniformity of the tunneling properties along the channel.

The proposed simulation methodology has shown a good agreement with experimental results. Therefore, the proposed simulation methodology, is a very valuable tool to investigate

non-homogeneous space distributed tunneling properties and other termo-magnetics effects on the gate tunneling current.

As a future work, in order to do more robust the gate tunneling model, more gate tunneling mechanims need to take into account; for instance trap assited tunneling.

Another future work can be focussed on studying the magnetic field effects having different orientations and directions. Until now, the VSP can handle 2D structures; however, in order to consider the application of magnetic fields in different directions, the VSP tool needs to handle with 3D structures. With the inclusion of this characteristic, device structures like FINFETs could be analyzed.

Finally, another future work is the implementation of a drain current model which incorporates the thermo-magnetic field effects. With this extension of the simulation tool, thermo-magnetic effects on the drain current by means of applying an external magnetic field perpendicular to the surface of the MOSFET could be done.

Bibliography

[1] Chaudhry A. and Roy J.N. *MOSFET Models, Quatum Mechanical Effects and Modeling Approaches: a Review.* Journal of Semiconductor Technology and Science, 10, (2010).

[2] International Technology Roadmap for Semiconductors Update 2012, Semiconductor Industry Association, San José, USA, Avaliable from ¡http://public.itrs.net¿

[3] N. Xu, L. T. Wang, A. R. Neureuther and T. J. King Liu. *Physically based modeling of stress-induced variation in nanoscale transistor performance..* IEEE Trans. Device Mat. Rel. 11, 3, (2001).

[4] X. Wang, A. R. Brown, N. Idris, S. Markov, G. Roy and A. Asenov. *Statistical threshold-voltage variability in scaled decananometer bilk HKMG MOSFETs: A full-scale 3D simulation scaling study.* IEEE Transactions on Electron Devices, 58, 8, 2011.

[5] E. A. Gutierrez-D, E. Pondigo-de los A., V. H. Vega, and F. Guarin, "Observation of Asymmetric Magnetoconductance in Strained 28-nm Si MOSFETs. " *IEEE Electron Device Letters*, 33, 254 (2012).

[6] E. Póndigo de los A., E. A. Gutierrez-D. , J. Molina, and F. Guarin, "Asymmetrical Magneto-Tunneling Conductance in MOSFETs Induced by Non-Homogeneous Space Mechanical Strain." *ESSDERC'2014 Conference*, September (2014).

[7] Hasse J. and Dietrich M.*Process Variations and Probabilistic Integrated Circuit Design*, Springer Science and Business Media, (2012).

[8] Schwierz Frank. *Graphene Transistors*, Nature Nanotechnology, 5, (2010).

[9] Chaudhry Amit. *Fundamentals of Nanoscaled Field Effect Transistors*, Springer, New York, (2013).

[10] Sverdlov Viktor. "Strain-Induced Effects in Advanced MOSFETs", *Computational Microelectronics*, 14, 2 (2011).

[11] Vasileska D., Mamaluy, D., Khan, H. R., Raleva, K., Goodnick, S. M. *Semiconductor Device Modeling*. Journal of Computational and Theoretical Nanoscience, 5, 1-32, (2008).

[12] Chang-Hoon Choi, Ki-Young Nam, Zhiping Yu, and Robert W. Dutton. "Impact of Gate Direct Tunneling Current on Circuit Performance: A Simulation Study".*IEEE Trans. Electron Devices* 48, 2823 (2001)

[13] E. Cassan,"On the reduction of direct tunneling leakage through ultrathin gate oxides by one-dimensional Schrödinger-Poisson solver" *J. Appl.Phys.*, 87, 7931 (2000).

[14] Juan C. Ranuárez, M. J. Deen, and Chih-Hung Chen, "A review of gate tunneling current in MOS devices." *Microelectronics reliability, Elsevier*, 46, 1939 (2005).

[15] Stanislav Markov, "Gate Leakage Variability in Nano-CMOS Technology". *PhD Dissertation*, Glasgow, (2010).

[16] Harrison Walter, "Tunneling from an Independent Particle point of View". *Physical Review*, 123, (1961).

[17] R. Tsu and L. Esaki, "Tunneling in a finite superlattice." *Applied Physics Letters*, 22, 562 (1973).

[18] Zhu Wei. "Vacuum Micro-Electronics". *Wiley*,36-40, (2001).

[19] . Splinger R. and Vianello M. "A survey on the Liouville-Green (WKB) approximation for linear difference equations on the second order"- *Proceedings of the second international conference on difference equations*, Hungary, (1998).

[20] Rana F., Tiwari S. and Buchanan D.A. "Self consistent modeling of accumulation layers and tunneling currents through very thin oxides". *Applied Physics Letters*, 69, (1997).

[21] Trellakis A, Galick T, Pacelli A and Ravaioli U. *Iteartion scheme for the solution of the two dimensional Schrödinger-Poisson equations in quantum structures* Journal of Applied Physics 81(12), June, (1997).

[22] Lo S.H,Buchanan D.A.and Taur Y. "Modeling and characterization, of quantization, polysilicon, depletion, and direct tunneling effects in MOSFETs with ultrathin oxides". *IBM Journal of Research and Development* 43, 3, May, (1999).

[23] A.F.J. Levi Applied Quantum Mechanics. Sec. Edition, Cambridge Univerity Press, (2006).

[24] C. Jirauschek. *Accuracy of Transfer Matrix Approaches for Solving the Effective Mass Schrodinger Equation.* Journal of Quantum Electronics IEEE., 45, 9, (2009).

[25] Janik T. and Majkusiak B. *Analysis of the MOS Transistor Based on the Self-Consistent Solution to the Schrodinger and Poisson Equations and the Local Mobility Model.* IEEE Transactions on Electron Devices. Vol. 45 No. 6, June (1998).

[26] Shih W., Wang E.X., Jallepalli S., Leon F., Maziar C.M.,and Tasch A.F. "Modeling gate leakage current in nMOS structures due to tunneling through an ultra thin oxide". *Solid State Electronics*, 42, (1998).

[27] Register L., Rosenbaum E. Yang K. "Analytic model for direct tunneling current in polycrystalline silicon gate metal oxide semiconductor devices". *Applied Physics Letters*, 74, (1999).

[28] Mundanai S., Fan Y., Ouyang Q., Tasch A. and Banerjee S. "Modeling of direct tunneling current through gate dielectrics stacks". *Transactions on Electron Devices, IEEE*, 47, (2000).

[29] Cai J. and Sah C. "Gate tunneling currents in ultra thin oxide metal oxide silicon transistor".*Journal of Applied Physics*, 89, (2001).

[30] Lee W. and Hu C. "Modeling CMOS Tunneling Currents through ultrathin gate oxide due to conduction and valence band electron ang hole tunneling". *Transactions on Electron Devices, IEEE*, 48, (2001).

[31] Pirovano A. et al. "Two dimensional quantum effects in nanoscale MOSFETs". *Transactions on electron devices*, 49, (2002).

[32] Curatola G and Iannaccone G.*NANOCAD2D: Two-dimensional code for the simulation of nanoelectronic devices and structures* Computantional Materials Science, 28 234-352, (2003).

[33] Curatola G., Fiori G. and Iannaccone G. *Modelling and simulation challenges for nanoscale MOSFETs in the ballistic limit.* Solid State Electronics Vol. 48, 581-587, (2004).

[34] Polizzi E and Abdallah B. *Subband decomposition approach for the simulation of quantum electron transport in nanosctructures* Journal of Computational Physics 202, 150-180, (2005).

[35] Driskill S.*Heterostructure Device Simulations using a Self-Consistent Schrodinger-Poisson Formulation.*REU Conference, (2004).

[36] Gildenblat G., Wang H., Chen T., Gu X. and Cai X. "SP: an advanced surface potential based compact model MOSFET model". *Journal of Solid State Circuits, IEEE*, 39, (2004).

[37] A. Gehring and S. Selberherr, "Modeling of tunneling current and gate dielectric reliability for nonvolatile memory devices" *IEEE Trans. Device Mat. Rel.*, 4, 306, (2004).

[38] Curatola G., Doornbos G., Loo J., Ponomarev Y. and Iannaccone G. *Detailed Modeling of Sub 100nm MOSFETs Based on Schrodinger DD Per Subband and Experiments and Evaluation of the Performance Gap to Ballistic Transport.* IEEE Transactions on Electronic Devices, Vol. 52 No. 8 , (2005).

[39] Trellakis A. Andlauer and Vogl P. *Efficient Solution of the Schrodinger-Poisson Equations in Semiconductor Device Simulation* Lecture Notes in Computer Science 3743, 602-609, (2006).

[40] Karner M., Gehring A.,Holzer S. Pourfath M.,Wagner M.,Goes W., Vasicek M., Baumgarter O., Kernstock C., Schnass G., Zeiler G., Grasser T., Kosina H. and Selberherr S. *A multi-purpose Schrodinger-Poisson Solver for TCAD applications.* Journal of Computational Electronics Vol. 6, pp. 179-182, (2007).

[41] Pourghaderi A.,Magnus W., Sorée B.,De Meyer K.,Meuris M. and Heyns M. *General 2D Schrodinger-Poisson solver with open boundary conditions for nano-scale CMOS transitors.* Journal of Computational Electronics. Vol. 7, 475-484, (2008).

[42] Soree B., Magnus W. and Pourtois G. "Analytical and self consistent quantum mechanical model for a surrounding gate MOS nanowire operate in JFET mode". *Journal of Computational Electronics*, 7, (2008).

[43] Cheng C, Lee J-H, Massoud H and Liu Q-H. *3-D self consistent Schrödinger-Poisson solver: the spectral element method* Journal of Computational Electronics 7, 337-341, (2008).

[44] Anderson C. "Efficient solution of the Schrödinger-Poisson equations in layered semiconductor devices". *Journal of computational physics*, 228, (2009).

[45] Esseni D. , Palestri P. and Selmi L. *Nanoscale MOS Transitors Semi- Classical Transport and Applications.* Cambridge, (2011).

[46] O. Baumgartner, Z. Stanojevic, K. Schnass, M. Karner and H. Kosina, "VSP-a quantum electronic simulation framework." *J. Comput. Electron.*, 12, 701 (2013).

[47] Popovic R.S. *Numerical Analysis of MOS Magnetic Field Sensors*. Solid State Electronics 28(7), 711-716,1984.

[48] Nathan A. *A Triple-drain MOSFET magnetic field sensor* Candian Journal of Physics. Vol. 63, 695-698,1985.

[49] Riccobenne C, Wachutka G, Burgler J and Baltes H.*Operating principle of dual collector magnetotransistor studied by two-dimensional simulation* IEEE Transactions on Electronic Devices 41(1), 1994.

[50] Lau J., Ko P. and Chan P. *Modelling of split-drain magnetic field-effect transistor MAGFET*. Sensors and Actuators A: Physical, Vol. 49, No. 3, 155-162, 1995.

[51] Puel Marjolaine. *Converge of the Schrödinger-Poisson system to the Euler equations under the influence of a large magnetic field*. Mathematical Modelling and Numerical Analysis,ESAIM: M2AN Vol 36 No 6, 2002.

[52] Rodríguez-Torres R.,Gutiérrez E.,Klima R. and Selberherr S. *Analysis of Split-Drain MAGFET* IEEE Transactions on Electron Devices, Vol. 15 No. 12, 2004.

[53] Birner, Hackenbuchner, Sabathil, Zandler, Majewski,Andlauer, Zibold,Morschl, Trellakis, Vogl. *Nextnano: General Purpose 3-D Simulations*.IEEE Transaction on Electronic Devices 54(9),2007

[54] Sudiarta W. and Geldart W. *Solving the Schrödinger Equation for a Charge Particle in a Magentic field using the Finite Difference Time Domain Method*. Computational Physics. Physics Letters A, 372(18),3145, Jan, (2008).

[55] Yosry E, Fikry W, El-henawy A and Marzouk M. *Compact Model of Dual-Drain MAGFETs Simulation*. International Journal of Electronics, Communications and Computer Engineering 1(2), 2009.

[56] Jiannis K. Pachos. "Introduction to Topological Quantum Computation" 14-36. *Cambridge University Press*, New York (2012).

[57] Sudiarta W. and Geldart W. *Solving the Schrödinger Equation for a Charge Particle in a Magentic field using the Finite Difference Time Domain Method.* Computational Physics. Physics Letters A, 372(18),3145, Jan, (2008).

[58] Levi A.F. *Applied Quantum Mechanics.* Cambridge, Second edition, (2006).

[59] Harrison P. *Quantum Wells, Wires and Dots.* Wiley Interscience, Second edition, UK, (2005).

[60] GTS Framework:
htto: //www.globalcad.com/en/products/gts-framework.html

[61] Chapra S. y Canale R. *Métodos Numéricos para Ingenieros.* México. Mc Graw Hill, (2001).

[62] Burden R. *Análisis numérico* México. International Thomson, (2007).

[63] Peiro J and Sherwin S. *Finite difference,finite element and finite volume methods for partial differential equations.* Handbook of Materials Modeling, Vol 1, (2005).

[64] D.C. Sorensen, R.B. Lehoucq, C. Yang, and K. Maschhoff. http://www.caam.rice.edu/software/ARPACK/, (2008).

[65] Karner M., Gehring A., Holzer S., Pourfath M., Wagner M., Goes W., Vasicek M., Baumgarter O., Kernstock C., Schnass K., Zeiler G., Grasser T., Kosina H., and Selberherr S. *A multi-purpose Schrödinger-Poisson Solver for TCAD applications.* Journal of Computantional Electronics 6: 179-182, (2007).

[66] Stanojević Zlatan. *Simulation of Carrier Transport in Ultra-Thin-Body Devices.* MS Dissertation.Technical University of Vienna. Institute for Microelectronics. June (2009).

[67] Stanojevic, Z., Karner, M. ; Schnass, K. ; Kernstock, C. ; Baumgartner, O. ; Kosina, H.*A versatile finite volume simulator for the analysis of electronic properties of nanostructures.* SISPAD, (2011).

[68] E. Póndigo de los Ángeles. "Experimental characterization and analysis of magneto-conductance performance of 28nm MOSFETs " *PhD Dissertation*, INAOE, 69-72 (2014).

[69] Y. Yu , "Fundamentals of Semiconductors." *Springer*, First Edition, 223 (1996).

[70] Slava V. Rotkin and Karl Hess, "Possibility of a metallic field-effect transistor." *Applied Physics Letters*, 84(16), 3139 (2004).

[71] Shue-Chue Shen, Jing-Bin Zhu, Yao-Ming Mu, and Pu-Lin Liu. "Wavefunction mixture and composition for hybridized Zeeman states of P in Si." *Physical Review B*, vol 49, no. 8, (1994).

[72] W. Lei,O. Wibbelhoff, C. Notthoff, B. Marquardt, D. Reuter, A.D. Wieck, A. Lorke. "Magnetic field induced modification of the wavefunctions in InAs quantum dots." *Physica E*, 40 (6) (2008).

[73] F. A. Chaves, D. Jiménez, F. J. García Ruiz, A. Godoy, and J. Suñe, "Accurate Calculation of Gate Tunneling Current in Double Gate and Single-Gate SOI MOS-FETs through Gate Dielectrics Stacks." *IEEE Trans. Electron Device*, 59 (10), 2589 (2012).

[74] Jean-Pierre Berenger, "A Perfectly Matched Layer Absorption of Electromagnetic Waves." *J. Comput. Physics*, 114 (2), 185 (1993).

[75] Nanofinder HE.
http://www.lotis-tii.com